
DEEP-MACROFIN: INFORMED EQUILIBRIUM NEURAL NETWORK FOR CONTINUOUS-TIME ECONOMIC MODELS

Yuntao Wu

Electrical and Computer Engineering
University of Toronto
Toronto, Ontario, Canada
winstonyt.wu@mail.utoronto.ca

Jiayuan Guo

Joseph L. Rotman School of Management
University of Toronto
Toronto, Ontario, Canada
guoflora5@gmail.com

Goutham Gopalakrishna

Joseph L. Rotman School of Management
University of Toronto
Toronto, Ontario, Canada
goutham.gopalakrishna@rotman.utoronto.ca

Zissis Poulos

School of Information Technology
York University
Toronto, Ontario, Canada
zpoulos@yorku.ca

May 15, 2025

ABSTRACT

In this paper, we present Deep-MacroFin, a comprehensive framework designed to solve partial differential equations, with a particular focus on models in continuous time economics. This framework leverages deep learning methodologies, including Multi-Layer Perceptrons and the newly developed Kolmogorov-Arnold Networks. It is optimized using economic information encapsulated by Hamilton-Jacobi-Bellman (HJB) equations and coupled algebraic equations. The application of neural networks holds the promise of accurately resolving high-dimensional problems with fewer computational demands and limitations compared to other numerical methods. This framework can be readily adapted for systems of partial differential equations in high dimensions. Importantly, it offers a more efficient ($5\times$ less CUDA memory and $40\times$ fewer FLOPs in **100D** problems) and user-friendly implementation than existing libraries. We also incorporate a time-stepping scheme to enhance training stability for nonlinear HJB equations, enabling the solution of **50D economic models**.

1 Introduction

Partial Differential Equations (PDEs) represent a class of mathematical equations that encapsulate the rates of change with respect to continuous variables. These equations are ubiquitous in the fields of physics and engineering, offering succinct insights into phenomena pertaining to acoustics, thermodynamics, electrodynamics, etc., where closed-form analytical solutions may not always be found. In the realm of macroeconomics and finance, PDEs are used to model and forecast complex phenomena like economic growth, inflation, interest rates, and asset prices. General equilibrium problems in these fields are typically governed by nonlinear elliptical PDEs [7, 8, 1, 17]. The ability to numerically solve PDE systems allows us to scrutinize the effects of parameter alterations on the equilibrium state.

Given the inherent complexity in deriving exact analytic solutions to PDEs, particularly for nonlinear PDE problems, researchers frequently resort to numerical techniques, such as the Finite Difference Method (FDM) [20, 6], and the Finite Element Method (FEM) [47, 36]. The fundamental concept behind these numerical solutions involves discretizing the continuous domain into a grid (mesh) of finite elements and approximating derivatives using differences between adjacent points. While these methods can yield accurate solutions with careful grid choices, they may encounter instability and high computational costs, particularly for higher-dimensional problems or complex physical systems [22, 24]. D’Avernas et al. demonstrate that standard FDM can fail when solving economic problems, even with only

two state variables [10]. Moreover, FDM is not scalable, due to the high nonlinearity of PDEs governing economic equilibrium models and the computational infeasibility of solving large linear systems when an implicit scheme is employed. However, these traditional numerical schemes provide insights into handling nonlinearity by introducing a transient time dimension [7, 8, 10, 11].

Deep learning, particularly deep neural networks, has been used for a variety of tasks across multiple domains, including regression, classification, and the generation of images and natural language [18]. Recently, the use of deep learning to solve partial differential equations (PDEs) has emerged as a promising alternative to traditional numerical solutions [42, 4, 31]. This approach leverages the theorem that neural networks can serve as universal function approximators [23]. The primary methodology involves Physics-Informed Neural Networks (PINNs), which optimize neural networks using PDEs as loss functions to approximate solutions [37, 38]. However, to the best of our knowledge, deep learning has not been extensively utilized to solve equilibrium problems in continuous time economics, compared to the PINN literature.¹ These problems typically involve optimizing Hamilton-Jacobi-Bellman (HJB) equations, which often lack classical smooth solutions [26, 45]. Additionally, they are coupled with a system of algebraic equations derived from market clearing conditions, binding constraints, and financial frictions. Solving such a system of PDEs can be numerically unstable, while neural networks could potentially offer improved approximations.

In this paper, we present Deep-MacroFin, a comprehensive framework for solving PDEs, with a specific focus on continuous-time economic models. Our approach offers several advantages over numerical methods: (1) it accommodates higher dimensionality with sparse sampling. Specifically, we demonstrate the ability to solve a 100-dimensional Laplace equation using 4.3GB CUDA memory, 12 GFLOPs, with an average epoch time of 0.16 seconds; (2) it handles differentiation more accurately without explicit discretization; and (3) once the problem is solved, the solution can be accurately extrapolated to a larger domain, free from grid space constraints. Furthermore, our methods outperform existing neural network techniques in several ways: (1) they offer simpler, more user-friendly implementation, with support for string and \LaTeX input; (2) they can readily solve various types of PDEs such as free boundary models; and (3) they allow for flexible initial / boundary conditions, allowing for a shift in learning regions and accommodating various boundary conditions in high dimensions. Finally, (4) we incorporate a time-stepping scheme from traditional numerical methods, inspired by [19], leading to more stable training in macro-finance models involving HJB equations. We solve economics models upto 50D with time-stepping scheme.

2 Related work

While several libraries exist for numerically solving PDEs, many either struggle with high-dimensional settings or are tailored to physical sciences rather than economics. Deep-MacroFin addresses this gap by offering a user-friendly, end-to-end solution for solving economic equilibrium models governed by PDEs. We benchmark our method against two representative libraries:

PyMacroFin [9]. This library targets macro-finance equilibrium models in continuous time, typically with one or two state variables, using finite difference methods and implicit schemes based on [7]. To address the nonlinearity of HJB equations, it reformulates them as auxiliary linear parabolic PDEs, solved through transient time iterations. However, PyMacroFin is limited in scope—it supports only low-dimensional problems and a narrow class of economic PDE systems. Numerical instability and the curse of dimensionality make it unsuitable for more general or higher-dimensional models. In some of our experiments, we implement finite difference methods directly, rather than relying on PyMacroFin.

DeepXDE [31]. This is a general-purpose PINN library for solving both forward and inverse PDE problems with given initial and boundary conditions. It has been successfully applied in areas such as option pricing [44] and some economic dynamics [15]. Despite its flexibility, DeepXDE struggles with high-dimensional problems and lacks tailored features for economic models, limiting its applicability to complex equilibrium systems (see Section 4).

3 Methodology

3.1 Problem formulation

Following [7, 8], we consider two types of agents: experts (e) and households (h), each with distinct consumption preferences and stochastic differential utility [12]. Time is continuous and the horizon is infinite. In equilibrium, (1) agents maximize expected utility subject to consumption, asset holdings, and budget constraints, and (2) markets clear. Let Z_t be a Brownian motion on a filtered probability space $(\Omega, \mathcal{F}, \{\mathcal{F}_t\}_{t \geq 0}, \mathbb{P})$. The exogenous state variable $x \in \mathbb{R}^n$

¹This area is still nascent, albeit growing over time.

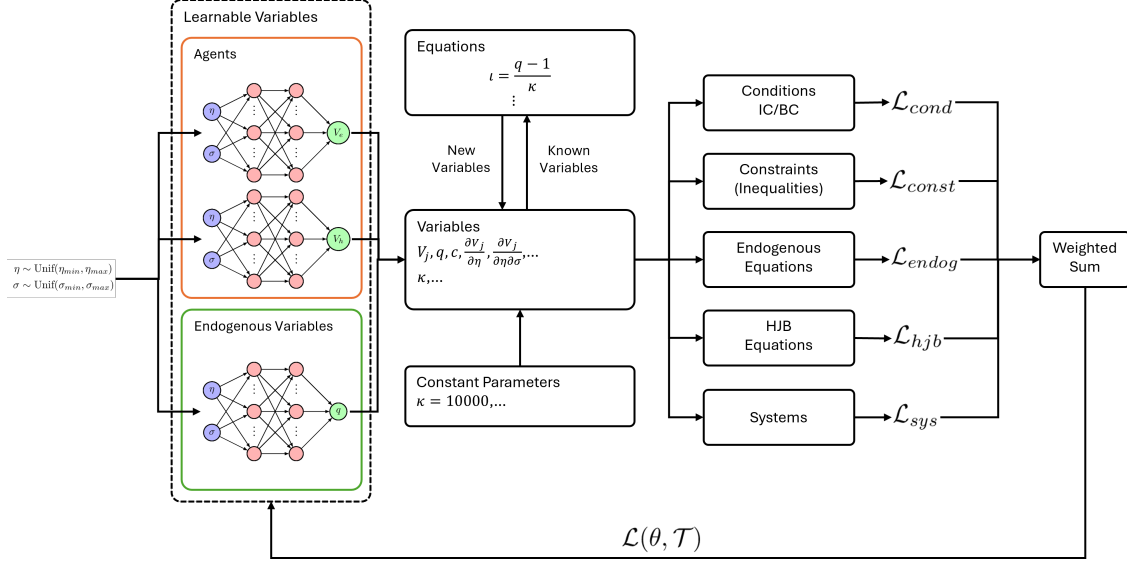


Figure 1: System overview. This model assumes the presence of two state variables: η (experts' wealth share) and σ (volatility), two agents: V_e (experts) and V_h (households), and one endogenous variable: q (price of the capital).

evolves according to the SDE:

$$dx_t = \mu_x dt + \sigma_x dZ_t \quad (1)$$

Each agent solves the following generic optimization problem:

$$\begin{aligned} \sup_{c_t^j} \mathbb{E}_T^{\mathbb{P}} \left[\int_T^\infty e^{-\rho t} u(c_t) dt \right], \\ \text{s.t. } f(x) \leq 0, g(x) = 0, \end{aligned}$$

where c_t denotes the consumption policy, and $u(c_t)$ the instantaneous utility. The constraint functions $f: \mathbb{R}^n \rightarrow \mathbb{R}^m$ and $g: \mathbb{R}^n \rightarrow \mathbb{R}^k$ encode budget, asset, and market clearing conditions, depending on endogenous variables such as capital prices q_t . Let $V_j(x)$ be the value function for agent j . Applying Itô's lemma yields the associated HJB equation:

$$\rho V_j(x) = \sup_c \left\{ u(c) + \nabla_x V_j^T \mu_x + \frac{1}{2} \sigma_x^T H_x(V_j) \sigma_x \right\}, \quad (2)$$

where $\nabla_x V_j$ and $H_x(V_j)$ are the gradient and Hessian of V_j , respectively. To approximate equilibrium quantities V , c , and q , we reformulate the optimization problem as a residual system:

$$\mathcal{E}_k(x; V_j, c_j, q; \nabla_x V_j, H(V_j); \lambda) = 0, \quad (3)$$

where $\lambda = \{a_e, a_h, \dots\}$ are parameters. The goal is to minimize the residuals, $\mathcal{L}_{\mathcal{E}_k} = \|\mathcal{E}_k\|^2$.

3.2 System design

Agent value functions V_j , and endogenous variables such as q , as outlined in the previous section, are approximated by neural networks, guided by endogenous and HJB equations. The framework also supports initial/boundary conditions, inequality constraints, and systems activated by constraints, enabling applications to basic PDEs, free boundary and variational problems. Let θ represent the neural network parameters and \mathcal{T} be the training data. The total loss is:

$$\mathcal{L}(\theta, \mathcal{T}) = \sum_i \lambda_i \mathcal{L}_i(\theta, \mathcal{T}), \quad (4)$$

which is a weighted sum of losses from all conditions, constraints, endogenous equations, and HJB equations, with each loss computation detailed in subsequent paragraphs. This weighted loss guides the neural network to learn the equilibrium solution without any assumption about the solution itself. Weights λ_i can be adjusted dynamically via learnable weights [43] or heuristic adaptation [5], though in this paper we manually select them for best empirical performance, as automatic methods proved less robust. Models that minimize $\mathcal{L}(\theta, \mathcal{T})$ ensures the approximated functions satisfy the specified equations and constraints. Figure 1 offers an overview of the system with two state variables. Further details on each component and the training process will be elaborated in the following paragraphs.

State variables and parameters State variables $X = (x_1, \dots, x_d) \in \mathbb{R}^d$ define the dimensionality and domain of the problem. In physical problems, they may represent space-time coordinates, while in economic problems, they could denote wealth shares or capital return volatility. Users can specify a domain $x_i \in [low_i, high_i]$, and values are sampled during training from user-defined distributions. Sampling can be uniform or follow an ergodic distribution, as in [16, 13]. Models are also governed by constant hyper-parameters. In the context of economic models, these could encompass factors such as relative risk aversion (γ), discount rate (ρ), etc. Different parameters can yield different solutions for the same underlying model. With neural networks, it is also possible to extend to more practical applications by treating fixed parameters as pseudo-variables and estimating their domains using real-world data.

Learnable variables Learnable variables, including agent value functions and endogenous variables, are unknown functions $f : \mathbb{R}^n \rightarrow \mathbb{R}^m$ to be approximated by neural networks. These learnable variables are modeled as configurable deep neural networks. The number of hidden units, hidden layers and outputs, and types of activation functions are customizable. Currently, Multi-Layer Perceptrons (MLPs) [18] and Kolmogorov-Arnold Networks (KANs) [28] are supported. While other architectures like DeepONet [30] can be integrated, they are outside the scope of this work.

The universal approximation theorem underlies MLP [23]. Automatic differentiation with batched Jacobian and Hessian enables precise and efficient calculation of derivatives [3, 35]. Furthermore, Sirignano and Spiliopoulos [42] shows that MLPs can approximate PDE solutions without knowing the exact form. In comparison, KAN is based on Kolmogorov-Arnold representation theorem. It is claimed to outperform MLP in terms of accuracy and interpretability. The interpretability stems from the symbolic formulas in KAN approximations, which can be easily extracted and evaluated. However, recent research suggests that KAN requires further improvements to match MLP in solving PDEs due to its lack of robustness and computational parallelism [41].

Equations The Equation module is used to define new variables. In economic models, the endogenous or HJB equations guiding the equilibrium are unlikely to directly depend on the agent value functions and endogenous variables. The Equation module provides a straightforward method to define intermediate variables. Given an equation $l = r(x)$, l is stored as a new variable in the system with an initial value of zero. During each iteration of training and testing, $r(x)$ is evaluated using known variables, and the resulting value is assigned to l . For example, the equation $\iota = \frac{q-1}{\kappa}$ in Figure 1 defines a new variable ι (investment). Its value is updated to $\frac{q-1}{\kappa}$ in each iteration. User-defined formulas can be raw Python code or L^AT_EX-based formula. The parsing of L^AT_EX is based on regular expression, independent of external libraries. This allows users to easily transfer their formulas from L^AT_EX documents to Python code.

Conditions Each learnable variable $v_i \in \{a_1, \dots, a_n, e_1, \dots, e_m\}$, either an agent value function or an endogenous variable, can be associated with specific conditions $\mathcal{C}(v_i, x) = 0$. In the context of mathematical or physical PDE problems, these conditions could represent initial value conditions $v_i(x_0) = v_{i0}$ or boundary value conditions $\mathcal{B}(v_i, x) = 0$, where $x \in \partial\Omega$, and $\Omega \subset \mathbb{R}^d$ is the problem domain. These conditions could be extended to any subsets $U \subset \Omega \cup \partial\Omega$ that require accurate approximation. These constraints are incorporated as a Mean Squared Error (MSE) over U : $\mathcal{L}_{cond} = \frac{1}{|U|} \sum_{x \in U} \|\mathcal{C}(v_i, x)\|_2^2$.

Endogenous equations The Endogenous Equation module is used to establish equalities that are required to pin down endogenous variables in the system. Typically, an endogenous equation takes the form of an algebraic (partial differential) equation $l(x) = r(x)$. Each endogenous equation is converted to a MSE loss over a batch of size B : $\mathcal{L}_{endog} = \frac{1}{B} \|l(x) - r(x)\|_2^2$.

HJB equations The HJB Equation module is used to inform the neural networks of the heterogeneous agent asset pricing models. Unlike PyMacroFin, which linearizes the HJB equation, Deep-MacroFin allows for direct input of HJB equations in the form of (2) to pin down each agent. As we aim for the optimal value of the HJB equation $\sup\{\text{HJB}(x)\}$ to be zero, the MSE loss can be computed over a batch of size B as: $\mathcal{L}_{hjb} = \frac{1}{B} \|\text{HJB}(x)\|^2$. The optimality conditions are computed using first-order conditions and are enforced using equations and endogenous equations. With different loss functions, this module can also be applied to solve variational problems as shown in Section 4.2.

Constraints The Constraint module is used to impose inequality conditions that restrict the solution space of the model. It enables the neural network to account for scenarios where valid solutions must lie within a specific subset of the full function space spanned by the network. For $l(x) \leq r(x)$, a rectified MSE is computed over a batch of size B : $\mathcal{L}_{const} = \frac{1}{B} \|\text{ReLU}(l(x) - r(x))\|_2^2$, where $\text{ReLU}(x) = \max(x, 0)$. Therefore, loss is only computed for $x \in B$, where $l(x) > r(x)$, i.e. when the constraint $l(x) \leq r(x)$ is violated. For $l(x) \geq r(x)$, the rectified MSE is computed as $\mathcal{L}_{const} = \frac{1}{B} \|\text{ReLU}(r(x) - l(x))\|_2^2$. In the case of strict inequalities, $l(x) > r(x)$ or $l(x) < r(x)$, an additional $\epsilon = 10^{-8}$ is added to the difference within ReLU to ensure strict inequalities.

Systems Systems are activated only when the binding constraints are satisfied. For a batch of inputs, both constraint-governed equations and endogenous equations are computed for each input in the batch. If an input does not satisfy the constraint, it is excluded from the loss computation. Equations are used to assign new variables and losses are computed based on the associated endogenous equations. Let $\mathbb{1}_{mask}$ be a vector of zeros and ones indicating which inputs in the batch meet the constraints. Then loss for a specific endogenous equation i in the system is $\mathcal{L}_{endog,i} = \frac{1}{\sum \mathbb{1}_{mask}} \langle (l-r)^2, \mathbb{1}_{mask} \rangle$, where $(l-r)^2$ is the element-wise square of $l-r$, and $\langle \cdot, \cdot \rangle$ denotes the inner product. Essentially, this is the MSE loss computed on mask-selected inputs. Let λ_i be the weight associated with each endogenous equation, and N be the number of endogenous equations attached to the system. The total loss of the system is $\mathcal{L}_{sys} = \sum_{i=1}^N \lambda_i \mathcal{L}_{endog,i}$.

3.3 Training

If the learnable variables are exclusively defined using MLPs, the neural networks can be trained using L-BFGS [27], Adam [25], or AdamW [29] algorithms. If any learnable variables are defined using KANs, then the KAN-customized L-BFGS algorithm [28] is employed. The neural networks are trained for a pre-defined number of epochs. To ensure reproducibility, the random seed is set to zero before training. Various training strategies can be employed depending on the problem context. A standard approach for a single epoch is outlined in Algorithm 1 in Appendix A. The objective is to approximate the optimal neural network parameters $\theta^* = \arg \min \mathcal{L}(\theta, \mathcal{T})$. Upon training completion, both the model with the lowest loss and the final epoch model are saved for analysis.

3.4 Time-stepping scheme

The standard training approach works well for many simple PDE systems but often fails for nonlinear HJB equations, as we demonstrate in Section 4.3. Traditional numerical schemes for macro-finance problems [7, 8, 10, 11, 19] introduce a transient but finite time dimension, analogous to value function iteration in discrete time. Rather than modeling an infinite-horizon economy, we consider a finite horizon $[0, T]$, with value functions and endogenous variables parametrized as $V_j(x, t)$ and $E_j(x, t)$. Given terminal conditions at T , we compute the equilibrium over $[0, T]$. By iteratively updating the boundary conditions, setting $V_j(x, T) \leftarrow V_j(x, 0)$ and $E_j(x, T) \leftarrow E_j(x, 0)$, equivalently taking $T \rightarrow \infty$, the behavior at $t = 0$ converges to the infinite-horizon equilibrium. This approach modifies the HJB equation via Itô’s lemma, introducing a time derivative and making the HJB quasi-linear:

$$\rho V_j(x, t) = \partial_t V_j(x, t) + u(c) + \nabla_x V_j^T \mu_x + \frac{1}{2} \sigma_x^T H_x(V_j) \sigma_x.$$

The implementation is outlined in Algorithm 2 in Appendix A.

4 Experiments

To evaluate Deep-MacroFin’s performance, we undertake various tasks: basic ODEs/PDEs, free boundary models derived from variational problems, and two standard economic problems. We benchmark with DeepXDE or numerical solutions. This section highlights main results, with detailed descriptions of each model and additional examples available in Appendix B. Low dimension models are trained on a Windows 11 machine with an i7-12700H CPU, RTX3070Ti Laptop GPU and 64GB RAM, while high dimension models are trained on a Linux RTX3090 machine. The backend uses PyTorch 2.4.1.

4.1 Basic PDEs and benchmarking with DeepXDE

We first evaluate basic boundary value problems with known analytic solutions to benchmark Deep-MacroFin against DeepXDE. Let $\Omega \subset \mathbb{R}^n$ be the domain with boundary $\partial\Omega$, and let L be a differential operator with boundary condition \mathcal{C} . We seek the unique solution u satisfying:

$$\begin{cases} L[u](x) = 0, x \in \Omega \\ \mathcal{C}(u, x) = 0, x \in \partial\Omega \end{cases}$$

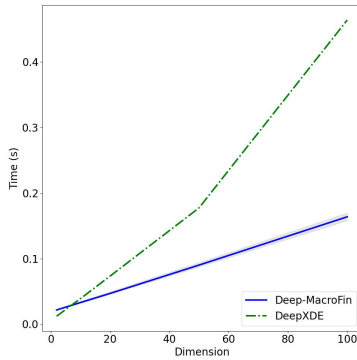
In low dimensions, we benchmark using Cauchy-Euler, diffusion, and Black-Scholes equations. For higher dimensions, we use Laplace equations with harmonic boundary conditions, where the solution is analytically known as $u(x) = g(x)$, $\forall x \in \Omega$ by the maximum principle. All low-dimensional models are trained with 50 random seeds using fixed configurations (Appendix B.1). DeepXDE uses the same setup as the baseline MLPs in Deep-MacroFin. We performed grid search for MLP hyperparameters, but the MSE variance across configurations was negligible ($\sim 10^{-6}$). In contrast,

KAN models were more sensitive to hyperparameters, and we manually selected the best-performing configuration. Table 1 reports mean and standard deviation of MSE, $\|u - \hat{u}\|_{L^\infty}$, $\|u - \hat{u}\|_{W^{1,\infty}}$, and $\|u - \hat{u}\|_{W^{2,\infty}}$. The Sobolev $W^{1,\infty}$ norm uses the max over batches of summed vector differences, and, and $W^{2,\infty}$ does the same with matrix differences. For low dimensions, errors are computed on fixed grids; for 100D Laplacian, on 10^5 random points. Our MLP implementation matches DeepXDE in MSE and $\|u - \hat{u}\|_{L^\infty}$ confirming robustness. However, DeepXDE wraps inputs as NumPy arrays for inference, preventing automatic differentiation for Jacobians and Hessians. Therefore, $W^{1,\infty}$ and $W^{2,\infty}$ norms are not reported for DeepXDE. These Sobolev norms are often large, as documented in prior work [46, 40], suggesting a future direction in designing architectures with better derivative accuracy. To evaluate the symbolic interpretability of KANs [28], we extract symbolic expressions and compare their errors to both the analytic solution (KAN Symbolic) and model predictions (KAN-KAN Symbolic). The symbolic errors align closely with original KAN errors, showing that KANs can accurately recover simple PDE solutions and potentially support efficient symbolic computation and root finding.

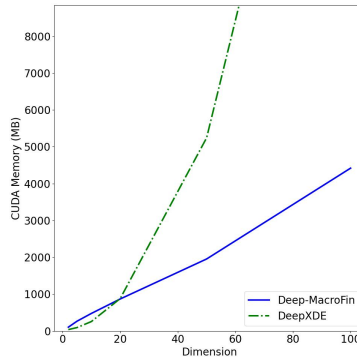
To test scalability, we experiment with dimensions $n \in \{2, 5, 10, 20, 50, 100\}$ on a Linux machine with RTX 3090 GPU. Models are 4-layer MLPs with 30 neurons per layer and SiLU activations, using a batch size of 1000. For each boundary hyperplane, 100 points are sampled, totaling 1000 + 200n points per training step. Figure 2 compares DeepXDE and Deep-MacroFin. Though Deep-MacroFin has slightly higher overhead in low dimensions (due to logging and derivative caching), it scales significantly better. It maintains stable runtime, memory usage, and FLOPs as dimensionality increases, requiring only 4.3GB CUDA memory (**5 \times** lower), 12 GFLOPs (**40 \times** lower), and 0.16s per epoch. Training for 100D model using Deep-MacroFin finishes within 30 minutes, while DeepXDE typically takes 75 minutes. DeepXDE’s rapidly increasing resource demands limit its scalability, which is a critical concern for high-dimensional economic applications like asset pricing models [32].

Table 1: Basic PDE errors

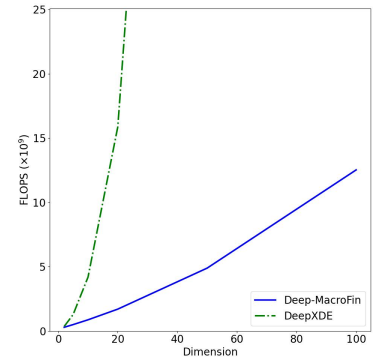
PDE	Model	MSE	$\ u - \hat{u}\ _{L^\infty}$	$\ u - \hat{u}\ _{W^{1,\infty}}$	$\ u - \hat{u}\ _{W^{2,\infty}}$
Cauchy-Euler	DeepXDE	$1.56 \times 10^{-5} (\pm 4.28 \times 10^{-5})$	$3.14 \times 10^{-3} (\pm 4.81 \times 10^{-3})$		
	MLP	$5.82 \times 10^{-6} (\pm 7.78 \times 10^{-6})$	$2.60 \times 10^{-3} (\pm 1.68 \times 10^{-3})$	$7.72 \times 10^{-3} (\pm 5.90 \times 10^{-3})$	$1.83 \times 10^{-1} (\pm 7.47 \times 10^{-2})$
	KAN	$2.79 \times 10^{-2} (\pm 2.48 \times 10^{-2})$	$4.29 \times 10^{-1} (\pm 3.10 \times 10^{-1})$	6.02 (± 4.16)	$5.43 \times 10^1 (\pm 3.17 \times 10^1)$
	KAN Symbolic	$8.14 \times 10^{-2} (\pm 1.91 \times 10^{-1})$	$5.46 \times 10^{-1} (\pm 3.86 \times 10^{-1})$	5.99 (± 4.23)	$5.03 \times 10^1 (\pm 3.05 \times 10^1)$
	KAN-KAN Symbolic	$5.13 \times 10^{-2} (\pm 1.92 \times 10^{-1})$	$2.65 \times 10^{-1} (\pm 2.81 \times 10^{-1})$	1.20 (± 1.32)	$1.04 \times 10^1 (\pm 2.40 \times 10^1)$
Diffusion	DeepXDE	$1.21 \times 10^{-5} (\pm 1.41 \times 10^{-5})$	$1.41 \times 10^{-2} (\pm 4.25 \times 10^{-3})$		
	MLP	$2.98 \times 10^{-5} (\pm 2.87 \times 10^{-5})$	$1.51 \times 10^{-2} (\pm 4.90 \times 10^{-3})$	$1.07 \times 10^{-1} (\pm 3.28 \times 10^{-2})$	$1.02 (\pm 2.84 \times 10^{-1})$
	KAN	$9.26 \times 10^{-4} (\pm 5.81 \times 10^{-6})$	$9.80 \times 10^{-2} (\pm 1.27 \times 10^{-3})$	$7.19 \times 10^{-1} (\pm 3.91 \times 10^{-2})$	$3.12 (\pm 4.47 \times 10^{-1})$
	KAN Symbolic	$9.26 \times 10^{-4} (\pm 6.40 \times 10^{-6})$	$9.81 \times 10^{-2} (\pm 1.33 \times 10^{-3})$	$7.19 \times 10^{-1} (\pm 3.90 \times 10^{-2})$	$3.12 (\pm 4.47 \times 10^{-1})$
	KAN-KAN Symbolic	$4.06 \times 10^{-9} (\pm 1.91 \times 10^{-8})$	$1.02 \times 10^{-4} (\pm 6.01 \times 10^{-5})$	$2.95 \times 10^{-4} (\pm 3.26 \times 10^{-5})$	$1.04 \times 10^{-3} (\pm 4.40 \times 10^{-5})$
Black-Scholes	DeepXDE	$2.40 \times 10^{-4} (\pm 1.05 \times 10^{-3})$	$3.79 \times 10^{-2} (\pm 4.42 \times 10^{-2})$		
	MLP	$1.20 \times 10^{-5} (\pm 5.87 \times 10^{-6})$	$1.53 \times 10^{-2} (\pm 3.60 \times 10^{-3})$	$8.38 \times 10^{-1} (\pm 1.11 \times 10^{-2})$	$1.10 \times 10^2 (\pm 7.15 \times 10^{-1})$
	KAN	$5.87 \times 10^{-5} (\pm 2.41 \times 10^{-5})$	$2.43 \times 10^{-2} (\pm 1.98 \times 10^{-3})$	$8.42 \times 10^{-1} (\pm 1.18 \times 10^{-2})$	$1.14 \times 10^2 (\pm 2.25 \times 10^{-1})$
	KAN Symbolic	$5.88 \times 10^{-5} (\pm 2.41 \times 10^{-5})$	$2.43 \times 10^{-2} (\pm 2.01 \times 10^{-3})$	$8.42 \times 10^{-1} (\pm 1.17 \times 10^{-2})$	$1.14 \times 10^2 (\pm 2.25 \times 10^{-1})$
	KAN-KAN Symbolic	$6.81 \times 10^{-9} (\pm 4.95 \times 10^{-9})$	$1.21 \times 10^{-4} (\pm 6.10 \times 10^{-5})$	$3.27 \times 10^{-4} (\pm 1.75 \times 10^{-4})$	$2.27 \times 10^{-3} (\pm 1.26 \times 10^{-3})$
Laplacian (100D) (Zero boundary)	DeepXDE	$2.26 \times 10^{-9} (\pm 1.33 \times 10^{-10})$	$2.52 \times 10^{-4} (\pm 4.37 \times 10^{-5})$		
	MLP	$9.14 \times 10^{-10} (\pm 4.99 \times 10^{-11})$	$1.36 \times 10^{-4} (\pm 2.31 \times 10^{-5})$	$1.36 \times 10^{-4} (\pm 2.31 \times 10^{-5})$	$1.36 \times 10^{-4} (\pm 2.31 \times 10^{-5})$
Laplacian (100D) (Summation boundary)	DeepXDE	$2.56 \times 10^{-2} (\pm 2.10 \times 10^{-4})$	$2.25 \times 10^{-1} (\pm 1.01 \times 10^{-2})$		
	MLP	$1.60 \times 10^{-3} (\pm 8.36 \times 10^{-5})$	$1.81 \times 10^{-1} (\pm 3.27 \times 10^{-2})$	$1.81 \times 10^{-1} (\pm 3.27 \times 10^{-2})$	$1.81 \times 10^{-1} (\pm 3.27 \times 10^{-2})$



(a) Training Time per Epoch



(b) Memory Usage



(c) FLOPs

Figure 2: Laplace equation benchmark

4.2 Free boundary problems

Many real-world problems in engineering, economics, and finance involve constraints and exhibit free boundaries. For example, in American option pricing, early exercise implies that the Black-Scholes equation holds only when the option price exceeds the payoff. Similar free-boundary structures appear in principal-agent models [39] and incomplete market equilibria [7]. Formally, the goal is to find the unique minimizer u of a functional $E[u]$ within a constrained subspace V of neural network-approximated functions:

$$\min_{u \in V} E[u] \quad \text{or equivalently,} \quad \min \{L[u](x), \mathcal{C}(u, x)\} = 0,$$

where $L[u]$ is the PDE derived from the variational problem and $\mathcal{C}(u, x)$ encodes the free boundary condition. Table 2 reports results for the Rochet–Choné model in 1D with active ($a = 0.5$) and inactive ($a = 2$) free boundaries; and the American option with dividend yield. Errors (MSE, L^∞ , and free boundary violation) are measured against numerical solutions from a projected SOR method on a fixed grid. Means and standard deviations are computed over 50 random seeds.

Our main focus is the incomplete market equilibrium (Proposition 4 in [7]), where the goal is to identify a critical wealth share η^ψ , beyond which the expert controls all market capital. When $\eta \in (0, \eta^\psi)$, agents can short-sell, leading to a nonlinear rise in the capital price q . When $\eta > \eta^\psi$, short-selling is prohibited, and q decreases linearly. Unlike other free-boundary problems (e.g., principal-agent and Black-Scholes), where transitions are smooth, the incomplete market model exhibits a discontinuous first derivative. To address this, we adopt an unwinding scheme: we solve two systems, one assuming $\psi < 1$, the other assuming $\psi = 1$, then locate the boundary where $\psi = 1$ in the first system and merge it with the second. Table 3 and Figure 3 show that both MLPs and KANs accurately approximate q and ψ . A key advantage of KAN is its ability to yield an analytical expression for η^ψ . For example: $\psi = -2.2823 + 3.7254 \exp(-1.0082(0.6741 - \eta)^2)$ implies $\eta^\psi \approx 0.3197$ for $\psi(\eta^\psi) = 1$. However, scaling KANs to higher dimensions remains challenging due to numerical instability with deeper or wider networks and limited parallelism. Also, as KAN becomes deeper or wider, the symbolic formula becomes more difficult to simplify and interpret.

Table 2: Free boundary models errors

PDE	Model	MSE	$\ u - \hat{u}\ _{L^\infty}$	Free Boundary Violation
Principal agent ($a = 0.5$)	MLP	$3.28 \times 10^{-4} (\pm 2.04 \times 10^{-4})$	$2.66 \times 10^{-2} (\pm 1.09 \times 10^{-2})$	0.00 (± 0.00)
	KAN	$2.23 \times 10^{-4} (\pm 2.14 \times 10^{-5})$	$2.07 \times 10^{-2} (\pm 1.48 \times 10^{-3})$	$1.39 \times 10^{-5} (\pm 9.92 \times 10^{-7})$
	KAN Symbolic	$2.30 \times 10^{-4} (\pm 2.10 \times 10^{-5})$	$2.16 \times 10^{-2} (\pm 1.57 \times 10^{-3})$	$9.27 \times 10^{-4} (\pm 2.99 \times 10^{-4})$
	KAN-KAN Symbolic	$2.35 \times 10^{-6} (\pm 1.38 \times 10^{-6})$	$5.79 \times 10^{-3} (\pm 1.35 \times 10^{-3})$	$9.27 \times 10^{-4} (\pm 2.99 \times 10^{-4})$
Principal agent ($a = 2$)	MLP	$4.76 \times 10^{-3} (\pm 4.42 \times 10^{-3})$	$7.75 \times 10^{-2} (\pm 2.77 \times 10^{-2})$	0.00 (± 0.00)
	KAN	$4.53 \times 10^{-5} (\pm 3.64 \times 10^{-5})$	$1.08 \times 10^{-2} (\pm 2.59 \times 10^{-3})$	$9.53 \times 10^{-3} (\pm 1.49 \times 10^{-3})$
	KAN Symbolic	$1.41 \times 10^{-3} (\pm 4.28 \times 10^{-3})$	$2.23 \times 10^{-2} (\pm 3.74 \times 10^{-2})$	$5.46 \times 10^{-3} (\pm 2.23 \times 10^{-3})$
	KAN-KAN Symbolic	$1.53 \times 10^{-3} (\pm 4.84 \times 10^{-3})$	$1.71 \times 10^{-2} (\pm 4.22 \times 10^{-2})$	$5.46 \times 10^{-3} (\pm 2.23 \times 10^{-3})$
Black-Scholes (American Option)	MLP	$6.49 \times 10^{-6} (\pm 5.58 \times 10^{-6})$	$5.47 \times 10^{-3} (\pm 2.76 \times 10^{-3})$	$2.92 \times 10^{-3} (\pm 1.68 \times 10^{-3})$
	KAN	$1.48 \times 10^{-5} (\pm 4.05 \times 10^{-6})$	$9.83 \times 10^{-3} (\pm 5.72 \times 10^{-4})$	$9.72 \times 10^{-3} (\pm 5.54 \times 10^{-4})$
	KAN Symbolic	$5.49 \times 10^{-5} (\pm 3.32 \times 10^{-6})$	$1.38 \times 10^{-2} (\pm 3.90 \times 10^{-4})$	$1.38 \times 10^{-2} (\pm 3.90 \times 10^{-4})$
	KAN-KAN Symbolic	$5.38 \times 10^{-5} (\pm 5.84 \times 10^{-6})$	$1.81 \times 10^{-2} (\pm 1.01 \times 10^{-3})$	$1.38 \times 10^{-2} (\pm 3.90 \times 10^{-4})$

Table 3: Brunnermeier & Sannikov

Model	MSE(q, \hat{q})	$\ q - \hat{q}\ _{L^\infty}$	MSE($\psi, \hat{\psi}$)	$\ \psi - \hat{\psi}\ _{L^\infty}$
MLP	$1.36 \times 10^{-6} (\pm 7.03 \times 10^{-7})$	$6.38 \times 10^{-5} (\pm 4.51 \times 10^{-5})$	$2.75 \times 10^{-3} (\pm 8.91 \times 10^{-4})$	$2.97 \times 10^{-2} (\pm 5.87 \times 10^{-3})$
KAN	$9.58 \times 10^{-8} (\pm 2.74 \times 10^{-7})$	$1.54 \times 10^{-5} (\pm 4.20 \times 10^{-5})$	$1.08 \times 10^{-3} (\pm 3.94 \times 10^{-4})$	$1.35 \times 10^{-2} (\pm 4.87 \times 10^{-3})$
KAN Symbolic	$7.84 \times 10^{-7} (\pm 1.05 \times 10^{-7})$	$1.78 \times 10^{-4} (\pm 1.58 \times 10^{-5})$	$4.50 \times 10^{-3} (\pm 2.74 \times 10^{-4})$	$7.25 \times 10^{-2} (\pm 3.98 \times 10^{-3})$
KAN-KAN Symbolic	$7.98 \times 10^{-7} (\pm 1.07 \times 10^{-7})$	$2.08 \times 10^{-4} (\pm 2.89 \times 10^{-5})$	$4.45 \times 10^{-3} (\pm 3.98 \times 10^{-4})$	$7.19 \times 10^{-2} (\pm 8.18 \times 10^{-3})$

4.3 Neoclassical growth model

The neoclassical growth model is a standard dynamic programming problem in macroeconomics. Its HJB equation is:

$$\rho V(k) = \max_c u(c) + V'(k)(k^\alpha - \delta k - c),$$

where $u(c) = \begin{cases} \frac{c^{1-\gamma}}{1-\gamma}, \gamma \neq 1 (\text{CRRA}) \\ \log(c), \gamma = 1 (\text{Log}) \end{cases}$ is the utility function. The FOC implies $u'(c) = V'(k)$. We parametrize both the value function V and consumption c using neural networks, and solve the system over the steady state $[k_{ss}, 2k_{ss}]$.

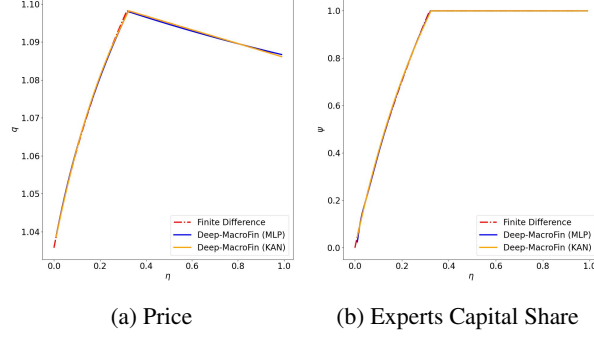


Figure 3: Brunnermeier & Sannikov: Red shows the finite difference solutions by PyMacroFin; blue shows the fitted solution by Deep-MacroFin with MLP; orange shows the fitted solution by KAN.

Table 4 reports errors across 20 random seeds for both MLP and KAN models. The neural network models approximate V and c well, with errors around 10^{-3} for both CRRA and log utility. However, KAN’s symbolic approximation often fails due to numerical instability, resulting in significantly higher errors in many trials. When extending the domain to $[0, 2k_{ss}]$, standard training struggles to approximate V and c accurately outside the steady state. To improve stability, we adopt the time-stepping scheme, by modifying the HJB equation to:

$$\rho V(k, t) = \max_c \partial_t V(k, t) + u(c) + \partial_k V(k, t)(k^\alpha - \delta k - c),$$

This modification reduces the mean squared error (MSE) across the entire domain to 10^{-5} , significantly improving accuracy, particularly outside the steady state, as shown in Figure 4. Furthermore, we extend this framework to a high-dimensional setting, with results presented in Appendix B.3.

Table 4: Neoclassical growth model steady state errors

PDE	Model	MSE (V)	$\ V - \hat{V}\ _{L^\infty}$	MSE (c)	$\ c - \hat{c}\ _{L^\infty}$
CRRA ($\gamma = 2$)	MLP	$9.54 \times 10^{-5} (\pm 1.33 \times 10^{-4})$	$1.17 \times 10^{-2} (\pm 7.25 \times 10^{-3})$	$2.03 \times 10^{-4} (\pm 1.93 \times 10^{-4})$	$2.83 \times 10^{-2} (\pm 1.39 \times 10^{-2})$
	KAN	$5.89 \times 10^{-5} (\pm 7.84 \times 10^{-5})$	$9.60 \times 10^{-3} (\pm 5.64 \times 10^{-3})$	$7.18 \times 10^{-5} (\pm 8.55 \times 10^{-5})$	$1.71 \times 10^{-2} (\pm 1.27 \times 10^{-2})$
Log ($\gamma = 1$)	KAN Symbolic	$2.97 (\pm 4.47)$	$1.78 (\pm 1.44)$	$9.12 \times 10^{-1} (\pm 3.81)$	$3.71 \times 10^{-1} (\pm 9.20 \times 10^{-1})$
	KAN-KAN Symbolic	$2.97 (\pm 4.46)$	$1.78 (\pm 1.43)$	$9.11 \times 10^{-1} (\pm 3.81)$	$3.61 \times 10^{-1} (\pm 9.17 \times 10^{-1})$
	MLP	$4.74 \times 10^{-5} (\pm 3.08 \times 10^{-5})$	$9.17 \times 10^{-3} (\pm 2.51 \times 10^{-3})$	$4.54 \times 10^{-5} (\pm 1.94 \times 10^{-5})$	$1.41 \times 10^{-2} (\pm 2.47 \times 10^{-3})$
	KAN	$6.82 \times 10^{-5} (\pm 8.24 \times 10^{-5})$	$1.03 \times 10^{-2} (\pm 5.05 \times 10^{-3})$	$1.80 \times 10^{-4} (\pm 1.87 \times 10^{-4})$	$2.12 \times 10^{-2} (\pm 1.01 \times 10^{-2})$
	KAN Symbolic	$1.64 (\pm 5.05)$	$5.57 \times 10^{-1} (\pm 1.36)$	$1.64 \times 10^6 (\pm 8.44 \times 10^5)$	$1.19 \times 10^3 (\pm 5.44 \times 10^2)$
	KAN-KAN Symbolic	$1.63 (\pm 5.05)$	$5.50 \times 10^{-1} (\pm 1.36)$	$1.64 \times 10^6 (\pm 8.44 \times 10^5)$	$1.19 \times 10^3 (\pm 5.44 \times 10^2)$

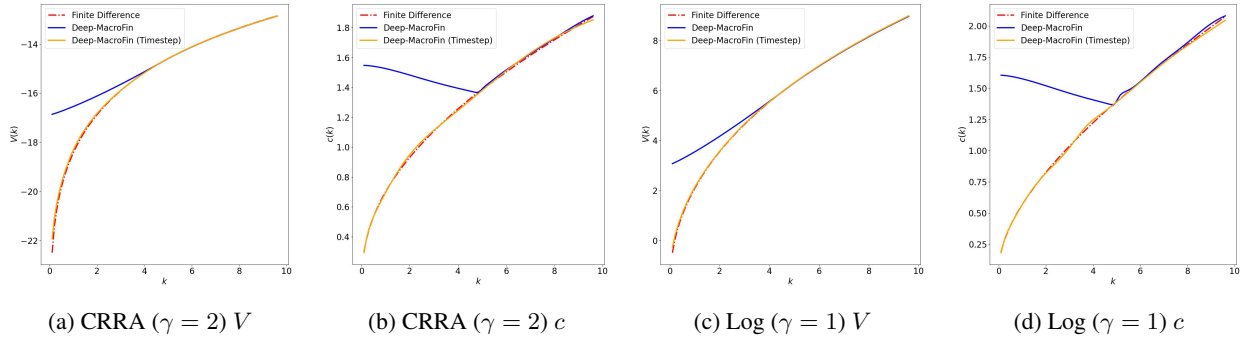


Figure 4: Neoclassical growth model global solution

4.4 Lucas orchard

In the final example, we study the Lucas orchard asset pricing problem [32]. For an economy with N trees, the state variables are the wealth shares z of each tree. We parametrize the value function κ with neural networks and solve the

HJB system using time-stepping for $N \in \{2, 5, 10, 20, 30, 40, 50\}$:

$$\begin{aligned}\mu^\kappa \kappa &= \partial_t \kappa + \nabla_z \kappa \mu_z + \frac{1}{2} \sigma_z^T H_z(\kappa) \sigma_z \\ \sigma^\kappa \kappa &= \nabla_z \kappa \sigma_z,\end{aligned}$$

where μ^κ and σ^κ also depend on price q of each tree, and μ_z, σ_z are geometric drift and diffusion of z . Figure 5 shows the results, with shaded regions indicating the $[5\%, 95\%]$ interval. FLOP tracking ends at $N = 40$ due to PyTorch profiler overhead, but the model scales efficiently, using only 8GB VRAM for $N = 50$, and can extend to higher dimensions. Validation against a numerical solution in 1D is provided in Appendix B.4. With time-stepping and ergodic sampling, the 50-tree model converges within 10 minutes.

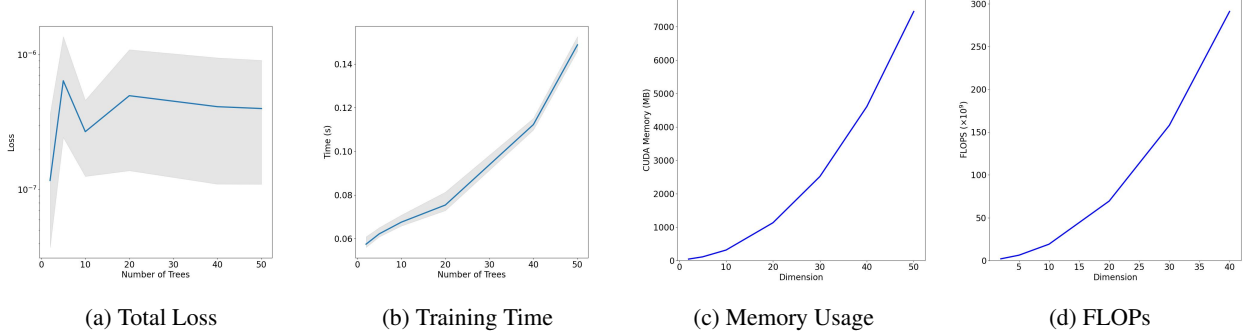


Figure 5: Lucas orchard benchmark

5 Conclusion

In this paper, we introduced Deep-MacroFin, a flexible and scalable framework for solving continuous-time economic models using deep learning. Designed to handle systems of differential equations, it outperforms existing libraries in both high-dimensional scalability and user customizability, offering a range of training algorithms and sampling strategies. We demonstrate that incorporating a time-stepping scheme from traditional numerical methods improves neural network solutions for continuous-time economic models with HJB equations. We also evaluated the performance of KANs. While their symbolic representations provide accurate approximations for simple PDEs and support analytical insights, they face challenges in scaling to higher dimensions due to numerical instability and limited parallelism. Our current limitations include the overhead from derivative pre-caching, leading to slight slowdowns in low dimensions, and the need for manual tuning of loss weights for improved convergence. Future work will focus on expanding the framework to more complex, high-dimensional, and dynamic economic models, as well as incorporating active learning and automated loss balancing to enhance training efficiency and accuracy.

References

- [1] Y. Achdou, J. Han, J.-M. Lasry, P.-L. Lions, and B. Moll. Income and wealth distribution in macroeconomics: A continuous-time approach. Working Paper 23732, National Bureau of Economic Research, 8 2017. URL <http://www.nber.org/papers/w23732>.
- [2] Y. Achdou, J. Han, J.-M. Lasry, P. L. Lions, and B. Moll. Income and Wealth Distribution in Macroeconomics: A Continuous-Time Approach. *The Review of Economic Studies*, 89(1):45–86, Jan. 2022. doi: 10.1093/restud/rdab002. URL <https://hal.science/hal-03886376>.
- [3] J. Ansel, E. Yang, H. He, N. Gimelshein, A. Jain, M. Voznesensky, B. Bao, P. Bell, D. Berard, E. Burovski, G. Chauhan, A. Chourdia, W. Constable, A. Desmaison, Z. DeVito, E. Ellison, W. Feng, J. Gong, M. Gschwind, B. Hirsh, S. Huang, K. Kalambarkar, L. Kirsch, M. Lazos, M. Lezcano, Y. Liang, J. Liang, Y. Lu, C. Luk, B. Maher, Y. Pan, C. Puhersch, M. Reso, M. Saroufim, M. Y. Siraichi, H. Suk, M. Suo, P. Tillet, E. Wang, X. Wang, W. Wen, S. Zhang, X. Zhao, K. Zhou, R. Zou, A. Mathews, G. Chanan, P. Wu, and S. Chintala. Pytorch 2: Faster machine learning through dynamic python bytecode transformation and graph compilation. In *29th ACM International Conference on Architectural Support for Programming Languages and Operating Systems, Volume 2 (ASPLOS ’24)*. ACM, Apr. 2024. doi: 10.1145/3620665.3640366. URL <https://pytorch.org/assets/pytorch2-2.pdf>.

- [4] N. Baker, F. Alexander, T. Bremer, A. Hagberg, Y. Kevrekidis, H. Najm, M. Parashar, A. Patra, J. Sethian, S. Wild, K. Willcox, and S. Lee. Workshop report on basic research needs for scientific machine learning: Core technologies for artificial intelligence. Technical report, USDOE Office of Science, 2 2019. URL <https://www.osti.gov/biblio/1478744>.
- [5] R. Bischof and M. Kraus. Multi-objective loss balancing for physics-informed deep learning, 2021. URL <http://rgdoi.net/10.13140/RG.2.2.20057.24169>.
- [6] W. Boyce and R. DiPrima. *Elementary Differential Equations and Boundary Value Problems*. Wiley, 2012. ISBN 9781118157381. URL https://books.google.ca/books?id=vf_qMgEACAAJ.
- [7] M. K. Brunnermeier and Y. Sannikov. A macroeconomic model with a financial sector. *American Economic Review*, 104(2):379–421, 2 2014. doi: 10.1257/aer.104.2.379. URL <https://www.aeaweb.org/articles?id=10.1257/aer.104.2.379>.
- [8] M. K. Brunnermeier and Y. Sannikov. Macro, money and finance: A continuous time approach. Working Paper 22343, National Bureau of Economic Research, 6 2016. URL <http://www.nber.org/papers/w22343>.
- [9] A. d’Avernas, D. Petersen, and Q. Vandeweyer. Macro-financial modeling in python: Pymacrofin, 2021. URL <https://adriendavernas.com/pymacrofin/index.html>.
- [10] A. d’Avernas, D. Petersen, and Q. Vandeweyer. A solution method for continuous-time general equilibrium models, 2021. URL <http://www.adriendavernas.com/papers/solutionmethod.pdf>.
- [11] S. Di Tella. Uncertainty shocks and balance sheet recessions. *Journal of Political Economy*, 125(6):2038–2081, 2017. doi: 10.1086/694290. URL <https://doi.org/10.1086/694290>.
- [12] D. Duffie and L. G. Epstein. Stochastic differential utility. *Econometrica*, 60:353–394, 1992. URL <https://api.semanticscholar.org/CorpusID:51787219>.
- [13] M. Ebrahimi Kahou, J. Fernández-Villaverde, J. Perla, and A. Sood. Exploiting symmetry in high-dimensional dynamic programming. Working Paper 28981, National Bureau of Economic Research, July 2021. URL <http://www.nber.org/papers/w28981>.
- [14] L. G. Epstein and S. E. Zin. Substitution, risk aversion, and the temporal behavior of consumption and asset returns: A theoretical framework. *Econometrica*, 57(4):937–969, 1989. ISSN 00129682, 14680262. URL <http://www.jstor.org/stable/1913778>.
- [15] B. Fan, E. Qiao, A. Jiao, Z. Gu, W. Li, and L. Lu. Deep learning for solving and estimating dynamic macro-finance models. *arXiv preprint arXiv:2305.09783*, 2023. URL <https://arxiv.org/abs/2305.09783>.
- [16] J. Fernández-Villaverde, G. Nuño, G. Sorg-Langhans, and M. Vogler. Solving high-dimensional dynamic programming problems using deep learning. Working paper, September 2020. URL https://maximilianvogler.github.io/My_Website/Deep_Learning.pdf.
- [17] M. Gomez. Asset prices and wealth inequality. 2017 Meeting Papers 1155, Society for Economic Dynamics, 2017. URL <https://EconPapers.repec.org/RePEc:red:sed017:1155>.
- [18] I. Goodfellow, Y. Bengio, and A. Courville. *Deep Learning*. MIT Press, 2016. URL <http://www.deeplearningbook.org>.
- [19] G. Gopalakrishna. Aliens and continuous time economies. Swiss Finance Institute Research Paper Series 21-34, Swiss Finance Institute, 2021. URL <https://EconPapers.repec.org/RePEc:chf:rpseri:rp2134>.
- [20] C. Grossmann, H.-G. Roos, and M. Stynes. *Numerical Treatment of Partial Differential Equations*. Springer Science & Business Media, 2007.
- [21] J. Han, A. Jentzen, and W. E. Solving high-dimensional partial differential equations using deep learning. *Proceedings of the National Academy of Sciences*, 115(34):8505–8510, 2018. doi: 10.1073/pnas.1718942115. URL <https://www.pnas.org/doi/abs/10.1073/pnas.1718942115>.
- [22] J. D. Hoffman and S. P. Frankel. *Numerical methods for engineers and scientists*. CRC Press, 2001.
- [23] K. Hornik, M. Stinchcombe, and H. White. Multilayer feedforward networks are universal approximators. *Neural Networks*, 2(5):359–366, 1989. ISSN 0893-6080. doi: [https://doi.org/10.1016/0893-6080\(89\)90020-8](https://doi.org/10.1016/0893-6080(89)90020-8). URL <https://www.sciencedirect.com/science/article/pii/0893608089900208>.
- [24] Y. Jaluria and S. N. Atluri. Computational heat transfer. *Computational Mechanics*, 14(5):385–386, 1994.
- [25] D. P. Kingma and J. Ba. Adam: A method for stochastic optimization. *ArXiv*, abs/1412.6980, 2017.
- [26] D. E. Kirk. *Optimal Control Theory: An Introduction*. Courier Corporation, 1970.

- [27] D. C. Liu and J. Nocedal. On the limited memory method for large scale optimization. *Mathematical Programming B*, 45(3):503–528, 1989.
- [28] Z. Liu, Y. Wang, S. Vaidya, F. Ruehle, J. Halverson, M. Soljačić, T. Y. Hou, and M. Tegmark. Kan: Kolmogorov-arnold networks. *arXiv preprint arXiv:2404.19756*, 2024.
- [29] I. Loshchilov and F. Hutter. Decoupled weight decay regularization. *ArXiv*, abs/1711.05101, 2019.
- [30] L. Lu, P. Jin, G. Pang, Z. Zhang, and G. E. Karniadakis. Learning nonlinear operators via deeponet based on the universal approximation theorem of operators. *Nature Machine Intelligence*, 3(3):218–229, 3 2021. ISSN 2522-5839. doi: 10.1038/s42256-021-00302-5. URL <http://dx.doi.org/10.1038/s42256-021-00302-5>.
- [31] L. Lu, X. Meng, Z. Mao, and G. E. Karniadakis. Deepxde: A deep learning library for solving differential equations. *SIAM Review*, 63(1):208–228, 2021. doi: 10.1137/19M1274067. URL <https://doi.org/10.1137/19M1274067>.
- [32] I. Martin. The lucas orchard. *Econometrica*, 81:55–111, 1 2013. ISSN 1468-0262. doi: 10.3982/ECTA8446. URL <https://onlinelibrary.wiley.com/doi/full/10.3982/ECTA8446><https://onlinelibrary.wiley.com/doi/abs/10.3982/ECTA8446><https://onlinelibrary.wiley.com/doi/10.3982/ECTA8446>.
- [33] R. J. McCann and K. S. Zhang. Comment on "ironing, sweeping, and multidimensional screening", 2023. URL <https://arxiv.org/abs/2311.13012>.
- [34] Q. Méridot and E. Oudet. Handling convexity-like constraints in variational problems, 2014. URL <https://arxiv.org/abs/1403.2340>.
- [35] A. Paszke, S. Gross, S. Chintala, G. Chanan, E. Yang, Z. DeVito, Z. Lin, A. Desmaison, L. Antiga, and A. Lerer. Automatic differentiation in pytorch. In *NIPS-W*, 2017.
- [36] A. Quarteroni and A. Valli. *Numerical Approximation of Partial Differential Equations*, volume 23. Springer Science & Business Media, 2008.
- [37] M. Raissi, P. Perdikaris, and G. E. Karniadakis. Physics informed deep learning (part i): Data-driven solutions of nonlinear partial differential equations. *arXiv preprint arXiv:1711.10561*, 2017.
- [38] M. Raissi, P. Perdikaris, and G. E. Karniadakis. Physics-informed neural networks: A deep learning framework for solving forward and inverse problems involving nonlinear partial differential equations. *Journal of Computational Physics*, 378:686–707, 2019.
- [39] J.-C. Rochet and P. Choné. Ironing, sweeping, and multidimensional screening. *Econometrica*, 66(4):783–826, 1998. ISSN 00129682, 14680262. URL <http://www.jstor.org/stable/2999574>.
- [40] S. Shen, T. Shao, K. Zhou, C. Jiang, F. Luo, and Y. Yang. Hod-net: High-order differentiable deep neural networks and applications. *Proceedings of the AAAI Conference on Artificial Intelligence*, 36(8):8249–8258, 2022. doi: 10.1609/aaai.v36i8.20799. URL <https://ojs.aaai.org/index.php/AAAI/article/view/20799>.
- [41] K. Shukla, J. D. Toscano, Z. Wang, Z. Zou, and G. E. Karniadakis. A comprehensive and fair comparison between mlp and kan representations for differential equations and operator networks. *arXiv preprint arXiv:2406.02917*, 2024. URL <https://arxiv.org/abs/2406.02917>.
- [42] J. Sirignano and K. Spiliopoulos. DGM: A deep learning algorithm for solving partial differential equations. *Journal of Computational Physics*, 2018. ISSN 10902716. doi: 10.1016/j.jcp.2018.08.029.
- [43] Y. Song, H. Wang, H. Yang, M. L. Taccari, and X. Chen. Loss-attentional physics-informed neural networks. *Journal of Computational Physics*, 501:112781, 2024. ISSN 0021-9991. doi: <https://doi.org/10.1016/j.jcp.2024.112781>. URL <https://www.sciencedirect.com/science/article/pii/S0021999124000305>.
- [44] X. Wang, J. Li, and J. Li. A deep learning based numerical pde method for option pricing. *Computational Economics*, 62:149–164, 2023. doi: <https://doi.org/10.1007/s10614-022-10279-x>.
- [45] J. Yong and X. Y. Zhou. *Stochastic Controls: Hamiltonian Systems and HJB Equations*. Springer, 1999.
- [46] Q. Zhu and J. Yang. A local deep learning method for solving high order partial differential equations. *arXiv preprint arXiv:2103.08915*, 2021. URL <https://arxiv.org/abs/2103.08915>.
- [47] P. Śolín. *Partial Differential Equations and the Finite Element Method*. John Wiley & Sons, 2005.

A Appendix: training algorithms

Algorithm 1 shows the basic training algorithm, similar to all standard training procedures. Algorithm 2 shows the training procedure for time-stepping scheme adopted from traditional numerical solutions to macro-finance model, as outlined in Section 3.4. In the time-stepping scheme, the initial guesses $\hat{V}_{i,\tau=0}$ and $\hat{E}_{i,\tau=0}$ can be set either as constants or based on precomputed guess function values. A good initial guess, closer to the true solution, may reduce the number of outer loop iterations, but it generally does not affect the overall convergence of the method.

Algorithm 1 Basic training algorithm (single step)

Input: Neural networks $\{a_1, \dots, a_n, e_1, \dots, e_m\}$, with parameters θ

- 1: Sample a batch of state variables $X = (x_1, \dots, x_d)$
 - 2: **for all** $v_i \in \{a_1, \dots, a_n, e_1, \dots, e_m\}$ **do**
 - 3: Compute $v_i(\theta, X)$, and all associated derivatives
 - 4: **for all** eq \in equations **do**
 - 5: Update variables defined by eq.lhs using eq.rhs
 - 6: Compute losses from conditions, constraints, endogenous / HJB equations and systems
 - 7: Compute the total loss $\mathcal{L}(\theta, \mathcal{T})$ with (4)
 - 8: Backward propagation and update θ to minimize $\mathcal{L}(\theta, \mathcal{T})$
-

Algorithm 2 Time-stepping scheme

Input: X : state variables with time t ,

$V_i : X \rightarrow \mathbb{R}$: agent value variables,

$E_j : X \rightarrow \mathbb{R}$: endogenous variables,

Output: Trained approximations \hat{V}_i, \hat{E}_j .

- 1: $\tau \leftarrow 0, \hat{V}_{i,\tau=0} = 1, \hat{E}_{i,\tau=0} = 1$ {Initialize as constant}
 - 2: **while** True **do**
 - 3: Sample $X = (x_0, \dots, x_n, t)$ uniformly random from domain (x_0, \dots, x_n are defined by the problem domain, $t \in [0, 1]$)
 - 4: Embed boundary conditions: $V_{i,\tau+1}(t=1) = \hat{V}_{i,\tau}, E_{i,\tau+1}(t=1) = \hat{E}_{i,\tau}$ {At maximum time, the functions should satisfy the value from the previous step}
 - 5: **while** True **do**
 - 6: Compute variables using neural networks, with $\frac{\partial V_i}{\partial t}$, and $\frac{\partial E_i}{\partial t}$ integrated.
 - 7: Compute loss on boundary conditions, endogenous equations, HJB equations and systems
 - 8: Compute total loss
 - 9: **if** iter \geq max_inner_loop OR inner loss converges **then**
 - 10: break
 - 11: $\hat{V}_{i,\tau+1} \leftarrow V_{i,\tau+1}(t=0), \hat{E}_{i,\tau+1} \leftarrow E_{i,\tau+1}(t=0), \tau \leftarrow \tau + 1$
 - 12: **if** iter \geq max_outer_loop OR \hat{V}_i, \hat{E}_i converge **then**
 - 13: break
-

B Appendix: model details and additional examples

B.1 Basic models

This appendix provides the details for models used in Section 4.1.

Cauchy-Euler

$$x^2 y'' + 6xy' + 4y = 0, \quad x \in [1, 2]$$

$$y(1) = 6, \quad y(2) = \frac{5}{4},$$

with solution $y = 4x^{-4} + 2x^{-1}$. The MSE is computed on 50 equally spaced inputs $x \in \{1.0, 1.02, \dots, 2.0\}$. A sample symbolic formula provided by KAN is:

$$y = -16.7436 + \frac{3.3016}{\left(-1 + \frac{0.0214}{\left(1 - \frac{0.0069}{0.0246x + 0.0034}\right)^4 + \frac{0.3063}{\left(-1 + \frac{0.0119}{(x + 0.1466)^4}\right)^4}}\right)^4}.$$

Diffusion

$$\begin{aligned} \frac{\partial y}{\partial t} &= \frac{\partial^2 y}{\partial x^2} - e^{-t}(\sin(\pi x) - \pi^2 \sin(\pi x)), \quad (x, t) \in [-1, 1] \times [0, 1] \\ y(x, 0) &= \sin(\pi x), \quad y(-1, t) = y(1, t) = 0. \end{aligned}$$

The solution is $y = e^{-t} \sin(\pi x)$. The MSE is reported over a 50×50 equally-spaced grid in the problem domain $(x, t) \in [-1, 1] \times [0, 1]$. A sample symbolic formula provided by KAN is:

$$\begin{aligned} &-3.2527 \exp(0.0735 \sin(2.3027x + 2.1834) + 0.0915 \exp(-0.9166t)) \\ &+ 0.2259 \exp(-0.8219 \sin(2.5074x + 3.8264) + 0.5529 \sin(0.9181t - 4.1949)) \\ &- 0.1011 \exp(-0.3498 \sin(3.8952x - 6.2036) + 1.2514 \sin(1.7026t + 1.8198)) \\ &+ 0.5222 \sin(3.8749 \sin(0.9643x + 8.3807) - 1.8474 + 0.6493 \exp(-2.3867t)) \\ &- 0.597 \sin(1.1602 \sin(1.848x - 0.7975) - 1.2157 \sin(1.1028t + 6.4883) + 3.8254) + 3.278. \end{aligned}$$

Note that the complexity of the KAN formula depends on the width and depth of the KAN layers. In this case, we use a 2-input, 1-output KAN model with a single hidden layer of width 5. The symbolic formula is a linear combination of five sine and exponential functions, with the inputs to each function being linear combinations of two sine and exponential functions, corresponding to the defined layer width. In comparison, the equation for Cauchy-Euler equation has a more nested structure, as it uses a 1-input, 1-output KAN model with two hidden layers.

Black-Scholes This section provides more details on the generalized N -asset Black-Scholes model:

$$\begin{aligned} \frac{\partial V}{\partial t} + rS \cdot \nabla V + \frac{\sigma^2}{2} S^T \rho \nabla_S^2 V S - rV &= 0, (S, t) \in [0, 1]^{N+1}, \\ V(S, T) &= \max \left\{ \frac{1}{n} \sum_{i=1}^N S_i - K, 0 \right\} \end{aligned}$$

where $S = (S_1, \dots, S_N)$ are the normalized underlying asset prices and t is normalized by time to maturity T . The constants are $\sigma = 0.2$ (volatility), $r = 0.05$ (risk-free rate), $K = 0.5$ (strike price), and ρ is a correlation matrix of the underlying asset processes, with $\rho_{ij} = \begin{cases} 1, i = j, \\ 0.5, i \neq j, \end{cases}$. This generalizes the one-asset model from [21], including the correlation factor and excluding default risk. The one-asset (2D) model has an analytic solution:

$$\begin{aligned} V(t, S) &= S\Phi(d_+) - Ke^{-r(T-t)}\Phi(d_-), \\ d_{\pm} &= \frac{\log(S/K) + (r \pm 0.5\sigma^2)(T-t)}{\sigma\sqrt{T-t}}, \end{aligned}$$

where Φ is the CDF of standard normal distribution. A sample symbolic formula provided by KAN is:

$$V(t, S) = -0.0654 + 0.5868 \exp\left(-8.7782 \left(0.52 + 0.9879 \exp\left(-0.9284(0.1783 - S)^2\right) - \exp(-0.0245t)\right)^2\right),$$

Laplacian

$$\begin{aligned} \Delta u &= 0, x \in \Omega = [0, 1]^n \\ \text{Zero boundary: } u(x) &= 0, x \in \partial\Omega, \\ \text{Summation boundary: } u(x) &= \sum_{i=1}^n x_i, x \in \partial\Omega \end{aligned}$$

Since the boundary conditions are harmonic, the maximum principle gives the analytical solution $u(x) = 0$ for zero boundary condition and $u(x) = \sum_{i=1}^n x_i$ for summation boundary condition.

Table 5 provides the exact values of mean epoch time (in seconds), memory usage (in MB), and FLOPs (floating-point operations) for the Laplace equation in 2, 5, 10, 20, 50, and 100 dimensions. The time is computed using Python’s built-in time package. Peak memory usage is recorded with `torch.cuda.max_memory_allocated()`, and FLOPs are estimated using the PyTorch Profiler². DeepXDE’s memory usage and FLOPs grow much faster than Deep-MacroFin’s. This demonstrates the potential of extending Deep-MacroFin to more complex economic models to higher dimensions.

Table 5: Time, memory and FLOPs benchmark with DeepXDE

N-dim	Mean Epoch Time (s)		CUDA Memory (MB)		FLOPs ($\times 10^9$)	
	Deep-MacroFin	DeepXDE	Deep-MacroFin	DeepXDE	Deep-MacroFin	DeepXDE
2	0.0216	0.0122	104.21	39.03	0.29	0.35
5	0.0259	0.0222	266.44	93.95	0.50	1.28
10	0.0330	0.0389	477.83	257.27	0.87	4.19
20	0.0469	0.0732	869.67	880.69	1.70	15.88
50	0.0901	0.1772	1955.26	5243.34	4.89	112.15
100	0.1637	0.4636	4421.12	21189.79	12.53	571.58

Model setup Table 6 shows the model setup.

Table 6: Model setup

PDE	Model	Hidden	#Params	Activation	Epochs	Optimizer	Learning rate
Cauchy-Euler	DeepXDE	[30]*4	2881	tanh	5000	Adam	10^{-3}
	MLP	[30]*4	2881	tanh	5000	Adam	10^{-3}
	KAN	[2,1]	94	SiLU	100	L-BFGS	1
Diffusion	DeepXDE	[30]*4	2911	tanh	5000	Adam	10^{-3}
	MLP	[30]*4	2911	tanh	5000	Adam	10^{-3}
	KAN	[5]	276	SiLU	100	L-BFGS	1
Black-Scholes	DeepXDE	[30]*4	2911	SiLU	5000	Adam	10^{-3}
	MLP	[30]*4	2911	SiLU	5000	Adam	10^{-3}
	KAN	[1]	56	SiLU	100	L-BFGS	1
Laplacian (100D)	DeepXDE	[30]*4	5851	SiLU	10000	Adam	10^{-3}
	MLP	[30]*4	5851	SiLU	10000	Adam	10^{-3}

B.2 Free boundary problems

This appendix provides the details for models used in Section 4.2.

Obstacle problem Let $\Omega \subset \mathbb{R}^n$ be a simply connected open set with smooth boundary $\partial\Omega$. Consider a smooth obstacle function $w \in C^2(\overline{\Omega})$ s.t. the solution u must satisfy $u \geq w$ for all $x \in \Omega$. The goal is to minimize the Dirichlet energy over Ω , subject to this inequality constraint and prescribed boundary conditions. The variational problem can be formulated as:

$$\begin{aligned}
\min_u E(u) &= \min_u \frac{1}{2} \int_{\Omega} \|\nabla u\|^2 \\
\text{s.t. } u(x) &= g(x), \quad x \in \partial\Omega \\
u(x) &\geq w(x), \quad x \in \Omega, w \in C^2(\overline{\Omega})
\end{aligned}$$

Define the admissible set:

$$V = \{v \in H^1(\Omega) : v \geq w \text{ in } \Omega; v = g \text{ on } \partial\Omega\}.$$

²https://pytorch.org/tutorials/recipes/recipes/profiler_recipe.html

The goal is to find $u \in V$ s.t. $E(u) \leq E(v)$, $\forall v \in V$. For simplicity, assume $g = 0$ constant.

Firstly, we derive the weak form and the associated Euler-Lagrange inequality for the variational problem. Let $u \in V$ be the minimizer, $v \in V$, $t \in \mathbb{R}$. Apply a perturbation to $E(u)$:

$$E(u + t(v - u)) = \frac{1}{2} \langle \nabla u + t \nabla(v - u), \nabla u + t \nabla(v - u) \rangle.$$

Since u is a minimizer, the derivative w.r.t. t at $t = 0$ should be non-negative:

$$\begin{aligned} \frac{d}{dt} E(u + t(v - u))|_{t=0} &= \frac{1}{2} \left(\langle \nabla(v - u), \nabla u + t \nabla(v - u) \rangle + \langle \nabla u + t \nabla(v - u), \nabla(v - u) \rangle \right) \Big|_{t=0} \\ &= \langle \nabla u + t \nabla(v - u), \nabla(v - u) \rangle|_{t=0} \\ &= \langle \nabla u, \nabla(v - u) \rangle \geq 0, \quad \forall v \in V \end{aligned}$$

Now, choose a specific variation $v = u + \eta\psi$ for $\eta \in \mathbb{R}$ small and $\psi \in C_c^\infty(\Omega)$ with $\psi \geq 0$ and $\psi = 0$ on $\partial\Omega$. Substituting into the inequality yields:

$$\begin{aligned} \langle \nabla u, \nabla(v - u) \rangle &= \int_{\Omega} \nabla u \nabla(v - u) = \int_{\Omega} \nabla u \nabla \eta \psi = \eta \int_{\Omega} \nabla u \nabla \psi \\ &= \eta \left(\int_{\partial\Omega} \nabla u \psi - \int_{\Omega} \nabla^2 u \psi \right) \\ &= -\eta \int_{\Omega} \nabla^2 u \psi = -\eta \langle \nabla^2 u, \psi \rangle \geq 0 \end{aligned}$$

In the region where $u = w$, $\eta > 0$ so that $v \geq w$ is satisfied, this requires $\langle \nabla^2 u, \psi \rangle \leq 0$ for all ψ , so $\nabla^2 u \leq 0$ a.e. in Ω . When $u > w$, η can be both positive or negative, for the inequality to hold for all ψ , we need $\nabla^2 u = 0$ a.e. in Ω . Thus, we obtain the following free boundary formulation of the obstacle problem:

$$\begin{aligned} \nabla^2 u &= 0, \quad x \in \Omega \cap \{u > w\} \\ \nabla^2 u &\leq 0, \quad x \in \Omega \cap \{u = w\} \\ u &\geq w, \quad x \in \Omega \\ u &= g, \quad x \in \partial\Omega \end{aligned}$$

In summary, the solution u lies above the obstacle w , is harmonic whenever it does not touch the obstacle ($u > w$), and it is superharmonic when it touches the obstacle ($u = w$). The interface between these two regions, where u transitions from being strictly greater than w to being equal to w , is known as the free boundary. We choose $w(x) = 1 - x^2$ in 1D, and $w(x) = 1 - x_1^2 - x_2^2$ in 2D and solve for u over $[-2, 2]^d$. The errors are computed over 50^d equally-spaced points on the domain with respect to numerical solutions from projected SOR method. In this example, MLP models perform better than KAN model, with smaller free boundary violation. Table 7 shows the errors, while Figure 6 shows the graphical results of the tested models.

Table 7: Obstacle problem errors

PDE	Model	MSE	$\ u - \hat{u}\ _{L^\infty}$	Free Boundary Violation
Obstacle (1D)	MLP	$1.21 \times 10^{-4} (\pm 8.58 \times 10^{-5})$	$2.02 \times 10^{-2} (\pm 5.47 \times 10^{-3})$	$2.02 \times 10^{-2} (\pm 5.47 \times 10^{-3})$
	KAN	$7.30 \times 10^{-4} (\pm 9.68 \times 10^{-5})$	$5.66 \times 10^{-2} (\pm 3.09 \times 10^{-3})$	$5.66 \times 10^{-2} (\pm 3.09 \times 10^{-3})$
	KAN Symbolic	$1.34 \times 10^{-3} (\pm 1.18 \times 10^{-4})$	$8.36 \times 10^{-2} (\pm 4.18 \times 10^{-3})$	$5.83 \times 10^{-2} (\pm 2.69 \times 10^{-3})$
	KAN-KAN Symbolic	$6.31 \times 10^{-4} (\pm 4.64 \times 10^{-5})$	$7.61 \times 10^{-2} (\pm 4.19 \times 10^{-3})$	$5.83 \times 10^{-2} (\pm 2.69 \times 10^{-3})$
Obstacle (2D)	MLP	$1.17 \times 10^{-3} (\pm 1.72 \times 10^{-3})$	$1.38 \times 10^{-1} (\pm 1.20 \times 10^{-1})$	$5.20 \times 10^{-2} (\pm 1.17 \times 10^{-2})$
	KAN	$8.94 \times 10^{-3} (\pm 2.64 \times 10^{-4})$	$3.04 \times 10^{-1} (\pm 7.72 \times 10^{-3})$	$1.88 \times 10^{-1} (\pm 4.34 \times 10^{-3})$
	KAN Symbolic	$8.84 \times 10^{-3} (\pm 2.52 \times 10^{-4})$	$3.24 \times 10^{-1} (\pm 8.03 \times 10^{-3})$	$1.69 \times 10^{-1} (\pm 4.65 \times 10^{-3})$
	KAN-KAN Symbolic	$1.43 \times 10^{-5} (\pm 1.46 \times 10^{-6})$	$2.91 \times 10^{-2} (\pm 1.41 \times 10^{-3})$	$1.69 \times 10^{-1} (\pm 4.65 \times 10^{-3})$

Principal agent problem Consider the Rochet–Choné formulation of the principal–agent problem [39, 33]. The principal offers a menu of products represented by types $y \in [0, \infty)^n$ with $y = 0$ representing the null product or outside option. Agents are heterogeneous and characterized by their type $x \in X \subset \mathbb{R}^n$, distributed according to a measure $\mu \ll \mathcal{L}$, where \mathcal{L} is the Lebesgue measure on \mathbb{R}^n . There exists a probability density function $f(x) = \frac{d\mu}{dx}$. The principal selects a price menu $v(y)$ to maximize profit, subject to the constraint that outside option has value $v(0) = 0$.

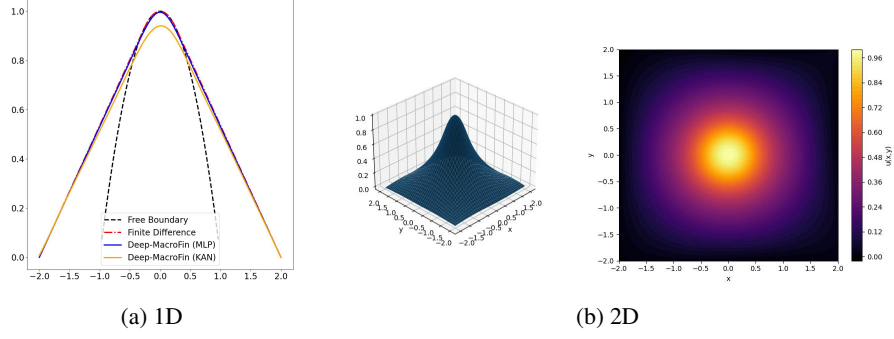


Figure 6: Obstacle problem

Producing a product of type y incurs a cost $c(y)$. The joint surplus generated from a transaction between an agent of type x and a product y is given by the bilinear form $b(x, y) = x \cdot y$. Agents choose products to maximize their utility:

$$u(x) = \sup_y b(x, y) - v(y),$$

which is the convex conjugate of the price function $v(y)$ w.r.t. the surplus $b(x, y)$. Assuming the optimal menu $y(x) = \nabla u(x)$, the principal's objective becomes the following variational problem:

$$\begin{aligned} \max_{u, \nabla u, \nabla^2 u \geq 0} \Phi(u) &= \max_{u, \nabla u, \nabla^2 u \geq 0} \int_X (b(x, y) - u(x) - c(y)) d\mu \\ &= \max_{u, \nabla u, \nabla^2 u \geq 0} \int_X (x \nabla u(x) - u(x) - c(\nabla u(x))) d\mu \end{aligned}$$

Choosing the quadratic production cost $c(y) = \frac{1}{2} \|y\|^2$, this becomes:

$$\max_{u, \nabla u, \nabla^2 u \geq 0} \Phi(u) = \max_{u, \nabla u, \nabla^2 u \geq 0} \int_X \left(x \nabla u(x) - u(x) - \frac{1}{2} \|\nabla u\|^2 \right) d\mu$$

In 1D with $X = [a, a+1]$, and uniform distribution $\frac{d\mu}{dx} = f(x) = \chi_{[a, a+1]} = \begin{cases} 1, & x \in [a, a+1] \\ 0, & \text{otherwise} \end{cases}$, we get the free boundary problem:

$$\begin{aligned} u'' &= 2, x \in [a, a+1] \cap \{u > 0\} \\ 0 \leq u'' &\leq 2, x \in [a, a+1] \cap \{u = 0\}, \text{ equivalently } u'' = 0 \\ u(a) &= 0, u'(a+1) = a+1, \end{aligned}$$

The free boundary is at $x = \frac{a+1}{2}$. For $a \leq 1$, the solution is

$$u(x) = \begin{cases} 0, & x \in [a, \frac{a+1}{2}] \\ (x - \frac{a+1}{2})^2, & x \in [\frac{a+1}{2}, a+1] \end{cases}.$$

When $a > 1$, the constraint $u \geq 0$ is inactive, and the solution becomes fully classical, $u(x) = (x - \frac{a+1}{2})^2 - (\frac{a-1}{2})^2$.

In economic sense, the parameter a is the lowest agent type considered by the principal. When $a < 1$, some low-type agents choose not to purchase (a buyer's market), and the region $\{x : u(x) = 0\}$ represents the set of excluded agents. The free boundary $x_0 = \frac{a+1}{2}$ is the threshold type that is indifferent to participating. When $a \geq 1$, all agents participate (a seller's market), and the solution does not have a free boundary. Table 8 reports the errors with respect to project SOR method in 1D.

In 2D, $X = [a, a+1]^2$. The free boundary is more difficult to be derived, and few numerical results are publicly available. In our implementation, we compute the functional Φ with simpson's method, set it as the HJB equation, and

directly minimize the variational integral with the following constraints to ensure convexity and curvature.

$$\begin{aligned} & \min \int_a^{a+1} \int_a^{a+1} \left(-x \nabla u(x) + u(x) + \frac{1}{2} \|\nabla u\|^2 \right) dx_1 dx_2 \\ & \text{s.t. } u \geq 0, \nabla u \geq 0, \det H(u) \geq 0 \\ & 0 \leq \frac{\partial^2 u}{\partial x_1^2} + \frac{\partial^2 u}{\partial x_2^2} \leq 3 \\ & u(0, 0) = 0 \end{aligned}$$

Figure 7 shows the solution in 2D using MLP, which aligns with numerical solutions as in [34]. KAN is not trained due to inefficient computation and lack of stability.

Table 8: Principal agent problem errors

PDE	Model	MSE	$\ u - \hat{u}\ _{L^\infty}$	Free Boundary Violation
Principal Agent ($a = 0$)	MLP	$1.71 \times 10^{-4} (\pm 1.24 \times 10^{-4})$	$2.13 \times 10^{-2} (\pm 9.89 \times 10^{-3})$	0.00 (± 0.00)
	KAN	$5.64 \times 10^{-5} (\pm 5.11 \times 10^{-6})$	$1.13 \times 10^{-2} (\pm 5.70 \times 10^{-4})$	$1.80 \times 10^{-6} (\pm 3.77 \times 10^{-8})$
	KAN Symbolic	$6.15 \times 10^{-5} (\pm 3.25 \times 10^{-6})$	$1.32 \times 10^{-2} (\pm 3.97 \times 10^{-4})$	$1.71 \times 10^{-3} (\pm 1.35 \times 10^{-3})$
	KAN-KAN Symbolic	$2.53 \times 10^{-6} (\pm 5.45 \times 10^{-6})$	$4.47 \times 10^{-3} (\pm 1.74 \times 10^{-3})$	$1.71 \times 10^{-3} (\pm 1.35 \times 10^{-3})$
Principal agent ($a = 0.5$)	MLP	$3.28 \times 10^{-4} (\pm 2.04 \times 10^{-4})$	$2.66 \times 10^{-2} (\pm 1.09 \times 10^{-2})$	0.00 (± 0.00)
	KAN	$2.23 \times 10^{-4} (\pm 2.14 \times 10^{-5})$	$2.07 \times 10^{-2} (\pm 1.48 \times 10^{-3})$	$1.39 \times 10^{-5} (\pm 9.92 \times 10^{-7})$
	KAN Symbolic	$2.30 \times 10^{-4} (\pm 2.10 \times 10^{-5})$	$2.16 \times 10^{-2} (\pm 1.57 \times 10^{-3})$	$9.27 \times 10^{-4} (\pm 2.99 \times 10^{-4})$
	KAN-KAN Symbolic	$2.35 \times 10^{-6} (\pm 1.38 \times 10^{-6})$	$5.79 \times 10^{-3} (\pm 1.35 \times 10^{-3})$	$9.27 \times 10^{-4} (\pm 2.99 \times 10^{-4})$
Principal agent ($a = 1$)	MLP	$1.12 \times 10^{-3} (\pm 1.10 \times 10^{-3})$	$4.18 \times 10^{-2} (\pm 2.02 \times 10^{-2})$	0.00 (± 0.00)
	KAN	$1.01 \times 10^{-4} (\pm 3.13 \times 10^{-5})$	$1.24 \times 10^{-2} (\pm 1.67 \times 10^{-3})$	$2.81 \times 10^{-3} (\pm 4.00 \times 10^{-4})$
	KAN Symbolic	$9.95 \times 10^{-5} (\pm 3.07 \times 10^{-5})$	$1.19 \times 10^{-2} (\pm 1.64 \times 10^{-3})$	$4.06 \times 10^{-4} (\pm 2.14 \times 10^{-4})$
	KAN-KAN Symbolic	$9.46 \times 10^{-7} (\pm 1.22 \times 10^{-7})$	$4.23 \times 10^{-3} (\pm 5.08 \times 10^{-4})$	$4.06 \times 10^{-4} (\pm 2.14 \times 10^{-4})$
Principal agent ($a = 2$)	MLP	$4.76 \times 10^{-3} (\pm 4.42 \times 10^{-3})$	$7.75 \times 10^{-2} (\pm 2.77 \times 10^{-2})$	0.00 (± 0.00)
	KAN	$4.53 \times 10^{-5} (\pm 3.64 \times 10^{-5})$	$1.08 \times 10^{-2} (\pm 2.59 \times 10^{-3})$	$9.53 \times 10^{-3} (\pm 1.49 \times 10^{-3})$
	KAN Symbolic	$1.41 \times 10^{-3} (\pm 4.28 \times 10^{-3})$	$2.23 \times 10^{-2} (\pm 3.74 \times 10^{-2})$	$5.46 \times 10^{-3} (\pm 2.23 \times 10^{-3})$
	KAN-KAN Symbolic	$1.53 \times 10^{-3} (\pm 4.84 \times 10^{-3})$	$1.71 \times 10^{-2} (\pm 4.22 \times 10^{-2})$	$5.46 \times 10^{-3} (\pm 2.23 \times 10^{-3})$

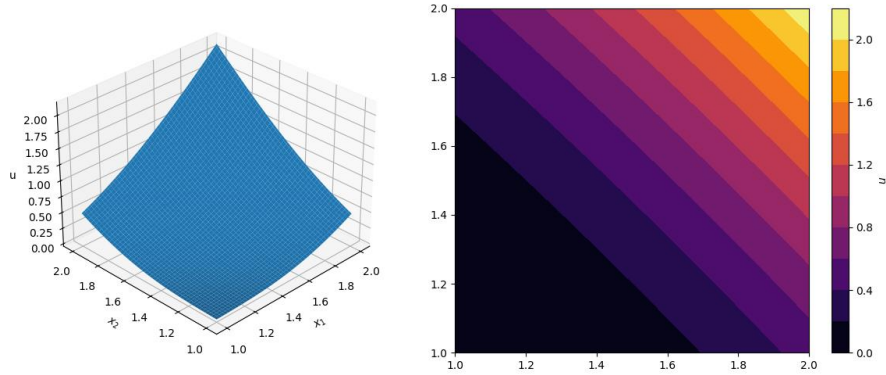


Figure 7: Principal agent problem

Black-Scholes (American option) The American option setup is similar to the basic European option. An additional dividend yield parameter q is added so that the free boundary is triggered. The goal is to solve for $V(S, t)$ with the following variational problem:

$$\begin{aligned} & \min \left\{ \frac{\partial V}{\partial t} + (r - q)S \frac{\partial V}{\partial S} + \frac{1}{2} \sigma^2 S^2 \frac{\partial^2 V}{\partial S^2} - rV, V - \max \{S - K, 0\} \right\} = 0 \\ & \text{s.t. } V(S, T) = \max \{S - K, 0\} \\ & V(0, t) = 0, V(1, t) = 1 - K \end{aligned}$$

The asset price S and time t are normalized to $[0, 1]$. The constants are $K = 0.3, r = 0.03, q = 0.08, \sigma = 0.4$. The errors are computed over $t = 0$.

Brunnermeier & Sannikov This model is based on Proposition 4 in [7] and is implemented in PyMacroFin, starting from an initial guess. Following the setup in [10], there are two endogenous variables, q and ψ . We use a quadratic investment function $\iota_t = \frac{q_t^2 - 1}{2\kappa}$, where κ is the investment rate. The constant parameters are provided in Table 9. The market clearing conditions and optimal portfolio choices lead to the following system of PDEs to solve when $\psi < 1$:

$$\begin{aligned} (r(1 - \eta) + \rho\eta)q &= \psi a_e + (1 - \psi)a_h - \iota \\ \sigma_t^q + \sigma &= \frac{\sigma}{1 - \frac{1}{q} \frac{\partial q}{\partial \eta} (\psi - \eta)} \\ (\sigma + \sigma_t^q)^2 \frac{q(\psi - \eta)}{\eta(1 - \eta)} &= a_e - a_h \end{aligned}$$

When $\psi = 1$, the system of PDEs simplifies to:

$$\begin{aligned} (r(1 - \eta) + \rho\eta)q &= a_e - \iota \\ \sigma_t^q + \sigma &= \frac{\sigma}{1 - \frac{1}{q} \frac{\partial q}{\partial \eta} (1 - \eta)} \end{aligned}$$

The functions q and ψ are approximated using neural networks. During training, σ_t^q is defined using $\sigma_t^q = \frac{\sigma}{1 - \frac{1}{q} \frac{\partial q}{\partial \eta} (\psi - \eta)} - \sigma$. Sum-of-squared errors are used for training, with a weight of 2 assigned to the endogenous equation involving $(\sigma + \sigma_t^q)^2$ for better convergence. The KAN models are 1-input and 1-output with no hidden dimensions so that it is easier to understand and demonstrate the symbolic formula.

Table 9: Free boundary model constant parameters

Parameter	Definition	Value
σ	exogenous volatility of capital	0.1
δ_e	depreciation rate of capital for experts	0.05
δ_h	depreciation rate of capital for households	0.05
a	productivity of experts	0.11
a_h	productivity of households	0.07
ρ	discount rate of experts	0.06
r	discount rate of households	0.05
κ	adjustment cost parameter	2

Model setup Table 10 shows the model setup for all free boundary models.

Table 10: Free boundary model setup

PDE	Model	Hidden	#Params	Activation	Epochs	Optimizer	Learning rate
Obstacle 1D	MLP	[50]*4	7801	SiLU	3000	Adam	10^{-3}
	KAN	[1]	38	SiLU	100	L-BFGS	10^{-3}
Obstacle 2D	MLP	[50]*4	7851	SiLU	3000	Adam	10^{-3}
	KAN	[1]	56	SiLU	100	L-BFGS	10^{-3}
Principle agent 1D	MLP	[50]*4	7801	SiLU	50000	Adam	10^{-3}
	KAN	[2]	75	SiLU	200	L-BFGS	1
Principle agent 2D	MLP	[50]*4	7851	SiLU	50000	Adam	10^{-3}
Black-Scholes (American option)	MLP	[30]*4	2911	SiLU	10000	Adam	10^{-3}
	KAN	[1]	56	SiLU	200	L-BFGS	1
Brunnermeier & Sannikov ($\psi < 1$)	MLP	[30]*4	2881	SiLU	10000	Adam	10^{-3}
	KAN	[]	19	SiLU	100	L-BFGS	1
Brunnermeier & Sannikov ($\psi = 1$)	MLP	[30]*4	2881	SiLU	2000	Adam	10^{-3}
	KAN	[]	19	SiLU	100	L-BFGS	1

B.3 Neoclassical growth

This appendix details the models and algorithms used in Section 4.3. The objective is to find the optimal consumption c and the value function V that solve the HJB equation:

$$\rho V(k) = \max_c u(c) + V'(k)(k^\alpha - \delta k - c),$$

The utility function is given by

$$u(c) = \begin{cases} \frac{c^{1-\gamma}}{1-\gamma}, \gamma \neq 1 (\text{CRRA}) \\ \log(c), \gamma = 1 (\text{Log}) \end{cases}$$

The first-order condition for optimality implies $u'(c) = V'(k)$. The steady state capital is at $k_{ss} = \left(\frac{\alpha}{\rho+\delta}\right)^{\frac{1}{1-\alpha}}$. Parameter values are listed in Table 11. We parametrize V and c using neural networks and solve the following system of PDEs:

$$\begin{aligned} c^{-\gamma} &= V'(k) \\ \rho V(k) &= u(c) + V'(k)(k^\alpha - \delta k - c) \\ V(k_{ss}) &= \begin{cases} \frac{(k_{ss}^\alpha - \delta k_{ss})^{1-\gamma}}{(1-\gamma)\rho}, \gamma \neq 1 \\ \frac{1}{\rho} \log(k_{ss}^\alpha - \delta k_{ss}), \gamma = 1 \end{cases}, \quad c(k_{ss}) = k_{ss}^\alpha - \delta k_{ss} \end{aligned}$$

Our results are compared against the benchmark numerical scheme from [2]. Initially, we solve the system over the domain $[k_{ss}, 2k_{ss}]$ using the basic algorithm. However, this basic approach does not generalize well to a broader domain. To address this, we adopt a time-stepping algorithm similar to value function iteration methods in numerical dynamic programming. The procedure is outlined in Algorithm 2. For faster convergence, the initial boundary condition for V is set to -18, and the initial guess for c is set to 1.5. Table 12 shows the model setup.

Table 11: Neoclassical growth model constant parameters

Parameter	Definition	Value
γ	relative risk aversion	$\gamma = 2/\gamma = 1$
ρ	time preference	$\rho = 0.05$
α	return to scale	$\alpha = 0.3$
δ	capital depreciation	$\delta = 0.05$

Table 12: Neoclassical growth model setup

PDE	Model	Hidden	#Params	Activation	Epochs	Optimizer	Learning rate
Basic (V)	MLP	[64]*4	12673	tanh	20000	Adam	10^{-3}
	KAN	[2,2]	149	SiLU	200	L-BFGS	1
Basic (c)	MLP	[32]*4	3265	tanh	20000	Adam	10^{-3}
	KAN	[2]	75	SiLU	200	L-BFGS	1
Timestepping (V)	MLP	[64]*4	12737	tanh	20×3000	Adam	10^{-3}
Timestepping (c)	MLP	[32]*4	3297	tanh	20×3000	Adam	10^{-3}

B.3.1 A high-dimensional multi-location dynamic capital allocation model

Following [16], we analyze a multi-location capital allocation model. Time is continuous and there are L locations. Each location l has a representative household with CRRA utility $u(c) = \frac{c^{1-\gamma}}{1-\gamma}$, and an idiosyncratic and exogenous

productivity z_l . The social planner solves the following optimization problem:

$$\begin{aligned}
\rho V(k, z) &= \max_{c, i, x} \sum_{l=1}^L u(c_l) + \nabla_k V^T (i - \delta k + x) + \nabla_z V^T \mu_z + \frac{1}{2} \sigma_z^T H_z(V) \sigma_z \\
\text{s.t.} \quad dz_l &= \left(-\nu \log(z_l) + \frac{\sigma^2}{2} \right) z_l dt + \sigma z_l dW_t^l \\
zk_l^\alpha &= c_l + i_l + 0.5\kappa_1 i_l^2 + 0.5\kappa_2 x_l^2 \\
\sum_{l=1}^L x_l &= 0
\end{aligned}$$

Table 13: Capital allocation model constant parameters

Parameter	Definition	Value
γ	relative risk aversion	$\gamma = 2$
ρ	time preference	$\rho = 0.04$
α	return to scale	$\alpha = 0.33$
δ	capital depreciation	$\delta = 0.07$
κ_1, κ_2	adjustment cost	$\kappa_1 = \kappa_2 = 1$
ν	autocorrelation of productivity	$e^{-\nu} = 0.8$
σ	variance of productivity	$\sigma = 0.33$

The constant parameters are given in Table 13. Define neural networks: $V : \mathbb{R}^{2L} \rightarrow \mathbb{R}^1$ (value function), $I : \mathbb{R}^{2L} \rightarrow \mathbb{R}^L$ (investments), $X : \mathbb{R}^{2L} \rightarrow \mathbb{R}^{L-1}$ (capital share). Note that the last dimension of capital share can be computed by $X_L = -\sum_{i=1}^{L-1} X_i$. Sample $z \in [0.5, 2.5]^L$, $k \in [2.5, 5.5]^L$. Compute:

$$\begin{aligned}
\mu_z &= \left(-\nu \log z + \frac{\sigma^2}{2} \right) z \\
\sigma_z &= \sigma z \\
C &= zk^\alpha - I - 0.5\kappa_1 I^2 - 0.5\kappa_2 X^2 \\
U &= \sum_{l=1}^L \frac{C_l^{1-\gamma}}{1-\gamma}
\end{aligned}$$

Taking FOC on I and X gives:

$$\begin{aligned}
\forall l \in \{0, 1, \dots, L\}, C_l^{-\gamma} * (1 + \kappa_1 I_l) - \frac{\partial V}{\partial k_l} &= 0 \\
\forall l \in \{0, 1, \dots, L-1\}, C_l^{-\gamma} (\kappa_2 X_l) - \frac{\partial V}{\partial k_l} &= C_L^{-\gamma} (\kappa_2 X_L) - \frac{\partial V}{\partial k_L}
\end{aligned}$$

Together with market clearing and HJB, we get a system of equation to solve:

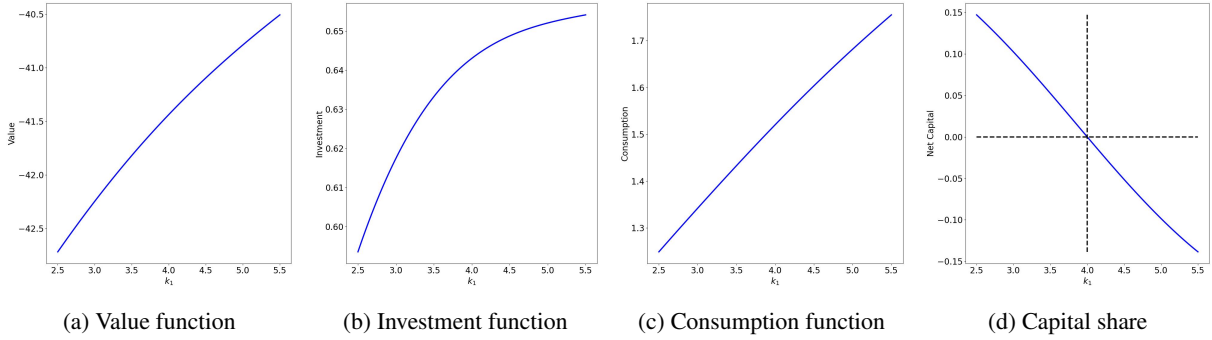
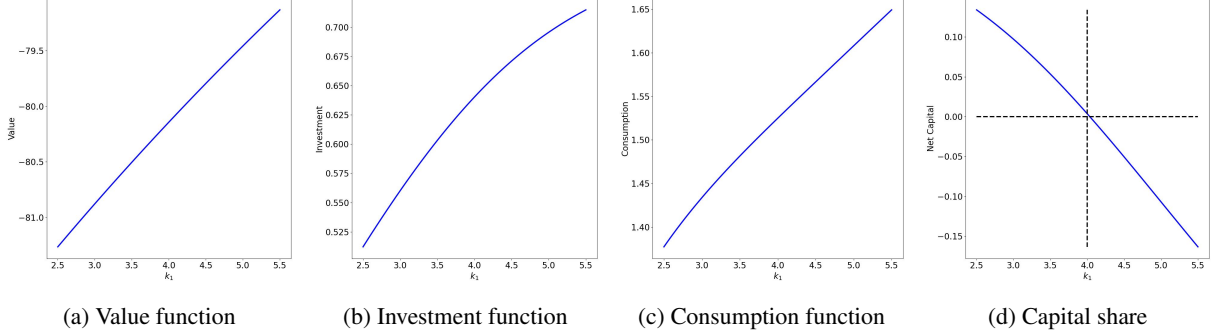
$$\begin{aligned}
C^{-\gamma} (1 + \kappa_1 I) - \nabla_k V &= 0 \\
\forall l \in \{0, 1, \dots, L-1\}, C_l^{-\gamma} (\kappa_2 X_l) - \frac{\partial V}{\partial k_l} &= C_L^{-\gamma} (\kappa_2 X_L) - \frac{\partial V}{\partial k_L} \\
\partial_t V + U + \nabla_k V^T (I - \delta k + X) + \nabla_z V^T \mu_z + \frac{1}{2} \sigma_z^T H(V) \sigma(z) &= \rho V
\end{aligned}$$

We train the model for $L = 2, 5, 25$ (4, 10, 50-dimension). Table 14 shows the model setup. The difference in the number of parameters is due to different output sizes. For 2- and 5-location models, we solve for the global solution, while for the 25-location model, we solve for the location solution for $k_1 \in [2.5, 5.5]$, $z_1 \in [0.5, 2.5]$, with $k_i = 4$, $z_i = 1.5$ for $i \in \{2, \dots, 25\}$. The 25-location model achieves early termination at the 36th timestep, with difference in error $< 10^{-4}$.

Figure 8, 9 and 10 show partial results for $L = 2, 5, 25$ respectively, displaying the value function, investment function, consumption function and net capital for Location 1. For visualization purposes, all non-displayed dimensions are fixed at their domain midpoints ($k_i = 4$ and $z_i = 1.5$). Value, investment and consumption functions have concave shapes with decaying growth rate as k increases, consistent with diminishing returns to capital accumulation. Net capital is decreasing and crosses 0 at $k_1 = 4$, since capital in all other locations is fixed at 4, location 1 imports capital for $k < 4$ and exports capital for $k > 4$. Note that in the original formulation in [16], the FOCs misses a factor of 2, or equivalently, the adjustment cost term $\kappa_1 i_l^2 + \kappa_2 x_l^2$ is missing a factor of 0.5. As a result, there is a discrepancy between our solution and theirs.

Table 14: Multi-location allocation model setup

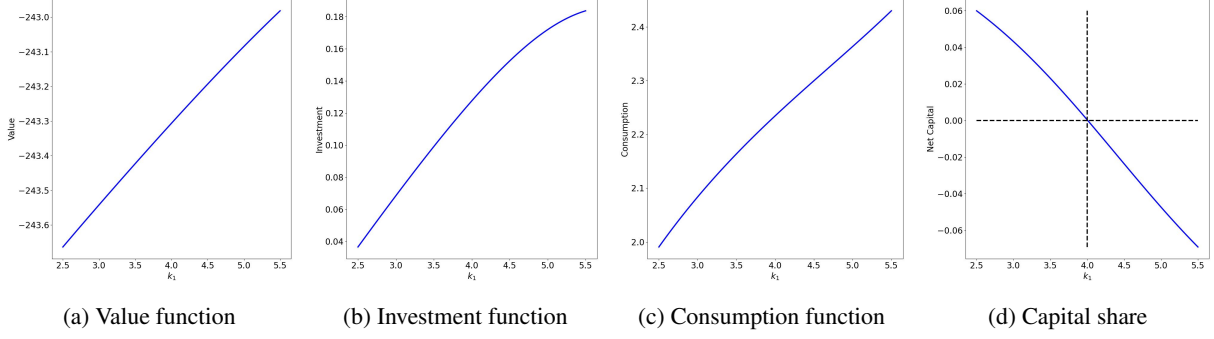
L	Variable	Hidden	#Params	Activation	Epochs	Optimizer	Learning rate
2	V, I, X	[64]*3, [30]*3, [30]*3	8769, 2102, 2071	tanh	20×10000	Adam	10^{-3}
5	V, I, X	[64]*3 for all	9153, 9413, 9348	tanh	50×10000	Adam	10^{-3}
25	V, I, X	[128]*3 for all	39809, 42905, 42776	tanh	50×10000	Adam	10^{-3}

Figure 8: 2-location capital allocation (HJB loss 2.47×10^{-5})Figure 9: 5-location capital allocation (HJB loss 2.63×10^{-4})

B.4 Lucas orchard

This appendix provides the details for models and algorithms used in Section 4.4. Consider an economy with N risky assets, each following a Lucas tree process. The dividend growth of each asset is assumed to be independent and identically distributed (i.i.d.) over time but potentially correlated across assets. An agent can hold multiple assets, but total wealth is constrained to equal 1. Therefore, we parametrize the agent's portfolio using $N - 1$ variables $z := (z_1, z_2, \dots, z_{N-1}) \in \mathbb{R}^{N-1}$, where z_i denotes the share of wealth invested in asset i . The value function $\kappa : \mathbb{R}^{N-1} \rightarrow \mathbb{R}^N$ represents the value associated with each tree. The dynamics of z are governed by a geometric Brownian motion:

$$dz_t = \mu^z z dt + \sigma^z z dW_t,$$

Figure 10: 25-location capital allocation (HJB loss 8.19×10^{-5})

where the components of z are normalized by the dividends y_i of each tree, which themselves follow geometric Brownian motions with constant drift μ^y and volatility σ^y . In our experiments, we set $\mu^{y_i} = \sigma^{y_i} = 0.01i$ for all models for illustration purpose. However, these parameters can be tuned to match the real-world scenarios. Each tree has a price q_j determined by the value function κ_j and the portfolio share z_j . The agent chooses asset weights w_j and consumption c_t , maximizing expected lifetime utility under a CRRA utility function with risk aversion parameter $\gamma = 5$ and discount rate $\rho = 0.05$:

$$\max_{c_t, w_t} \mathbb{E} \left[\int_0^\infty e^{-\rho t} \frac{c_t^{1-\gamma}}{1-\gamma} dt \right]$$

We define the full wealth share vector $\bar{z} = (z_1, \dots, z_{N-1}, 1 - \sum_{i=1}^N z_i)$, and denote by $\mu^{\bar{z}}$ and $\sigma^{\bar{z}}$ the corresponding drift and diffusion coefficients. We then compute the following variables in the equilibrium:

$$\begin{aligned} q &= \frac{\bar{z}}{\kappa} \\ \mu^{z_i} &= \mu^{y_i} - \mu^y \cdot \bar{z} + \sigma^y \cdot \bar{z} (\sigma^y \cdot \bar{z} - \sigma^{y_i}) \\ \sigma^{z_i} &= \sigma^{y_i} - \sigma^y \cdot \bar{z} \\ \mu_z &= \mu^z \times z \\ \sigma_z &= \sigma^z \times z \\ \mu_{z_N} &= - \sum_{i=1}^{N-1} \mu_{z_i} \\ \sigma_{z_N} &= - \sum_{i=1}^{N-1} \sigma_{z_i} \\ \mu^{z_N} &= \frac{\mu_{z_N}}{z_N} \\ \sigma^{z_N} &= \frac{\sigma_{z_N}}{z_N} \\ \mu^q &= \frac{1}{q} \times \left(\nabla_z q \mu_z + \frac{1}{2} (\sigma_z)^T H_z(q) \sigma_z \right) \\ \sigma^q &= \frac{1}{q} \times (\nabla_z q \sigma_z) \\ r &= \rho + \gamma \mu^y \cdot \bar{z} - \frac{1}{2} \gamma (\gamma + 1) (\bar{z})^2 \cdot (\sigma^y)^2 \\ \zeta &= \gamma \bar{z} \cdot \sigma^y \\ \mu^\kappa &= \mu^{\bar{z}} - \mu^q + \sigma^q \times (\sigma^q - \bar{z}) \\ \sigma^\kappa &= \sigma^{\bar{z}} - \sigma^q \end{aligned}$$

Then we solve for κ with the following HJB equations:

$$\begin{aligned}\mu^\kappa \kappa &= \partial_t \kappa + \nabla_z \kappa \mu_z + \frac{1}{2} \sigma_z^T H_z(\kappa) \sigma_z \\ \sigma^\kappa \kappa &= \nabla_z \kappa \sigma_z,\end{aligned}$$

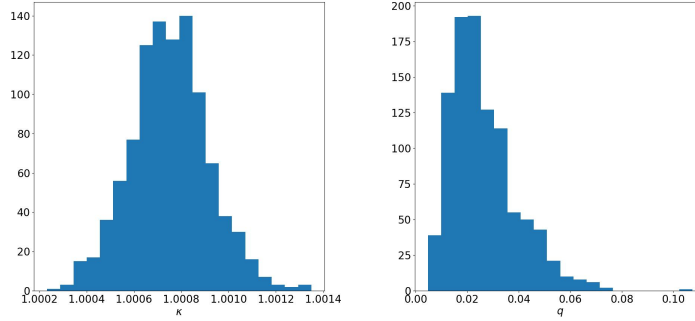
During training, we sample from the ergodic distributions of dividends, with

$$y_i \sim \text{LogNormal}(\mu^{y_i}, \sigma^{y_i})$$

and then normalize to obtain the portfolio shares z_i . κ is parametrized by 4-layer MLP with 80 hidden neurons in each layer. We use Adam optimizer with learning rate $\alpha = 5 \times 10^{-4}$. Table 15 reports the errors between our solution and the PyMacroFin benchmark in the 1D case. The value function κ is expected to be around 1, and since $q_i = \frac{z_i}{\kappa_i}$, under ergodic distribution, $q_i \approx \frac{1}{N}$ for N -tree models. Figure 11 shows the distribution of κ and q over the ergodic distribution, confirming the accuracy of our method.

Table 15: 2-Tree validation

	κ_1	κ_2	q_1	q_2
MSE	$3.93 \times 10^{-5} (\pm 3.21 \times 10^{-5})$	$3.96 \times 10^{-5} (\pm 3.23 \times 10^{-5})$	$1.82 \times 10^{-5} (\pm 1.58 \times 10^{-5})$	$1.33 \times 10^{-5} (\pm 1.50 \times 10^{-5})$
$\ \cdot\ _{L^\infty}$	$1.16 \times 10^{-2} (\pm 4.79 \times 10^{-3})$	$1.16 \times 10^{-2} (\pm 4.96 \times 10^{-3})$	$9.47 \times 10^{-3} (\pm 5.67 \times 10^{-3})$	$8.80 \times 10^{-3} (\pm 5.28 \times 10^{-3})$



(a) κ (b) q

Figure 11: 50-Tree Distribution

B.5 One-Dimensional Economic Model

This appendix provides the model details and results for another one dimensional economic model that numerical methods like PyMacroFin fails to solve due to singular matrix. Let $j \in \{h, e\}$ index two types of agents, where h represents households and i represents experts (intermediaries). We use i here to avoid the confusion with e for η in the code.

B.5.1 Ito's Lemma Derivations

Let Z_t be a Brownian motion on $(\Omega, \mathcal{F}, \{\mathcal{F}_t\}_{t \geq 0}, \mathbb{P})$. The evolution of the capital is given by

$$\frac{dk_t}{k_t} = (\Phi(\iota_t) - \delta)dt + \sigma dZ_t, \quad (5)$$

where δ and σ represent depreciation rate and volatility of capital, respectively. $\Phi(\cdot)$ is a functional form for the investment function ι_t . Experts finance their holdings by short-selling the risk-free asset to households, assuming there are no transaction costs, and the agents are price-takers. The price of capital q_t , has dynamics:

$$\frac{dq_t}{q_t} = \mu_t^q dt + \sigma_t^q dZ_t. \quad (6)$$

Capital returns dr_t^{kj} are based on dividend yield $\frac{a_j - \iota_t}{q_t} dt$ and capital gain $d(q_t k_t)$. The aggregate amount of capital is K_t , and the economy's aggregate net worth is $q_t K_t$. Let the aggregate net worth of experts be w_t^i . Experts' wealth share, η_t , is $\eta_t = \frac{w_t^i}{q_t K_t} \in [0, 1]$.

Given the dynamics of k_t^a (capital), q_t^a (price of capital), ξ_t^j (agent value function) and state variable η_t :

$$\frac{dk_t^a}{k_t^a} = (\mu^a + \Phi(\iota_t^a))dt + \sigma^a dZ_t^a \quad (7)$$

$$\frac{dq_t^a}{q_t^a} = \mu_t^{qa} dt + \sigma_t^{qa} dZ_t^a, \quad (8)$$

$$\frac{d\xi_t^j}{\xi_t^j} = \mu_t^{\xi j} dt + \sigma_t^{\xi ja} dZ_t^a, \quad (9)$$

$$\frac{d\eta_t}{\eta_t} = \left(\underbrace{(1 - \eta_t)(\mu_t^{ni} - \mu_t^{nh}) + (\sigma_t^{na})^2 - \sigma_t^{nia} \sigma_t^{na}}_{\mu_t^\eta} \right) dt + \underbrace{(1 - \eta_t)(\sigma_t^{nia} - \sigma_t^{nha})}_{\sigma_t^{\eta a}} dZ_t^a, \quad (10)$$

where Z_t^a is a standard Brownian motion on $(\Omega, \mathcal{F}, \{\mathcal{F}_t\}_{t \geq 0}, \mathbb{P})$. dZ_t^a is a Wiener process (with $\mu = 0$, $\sigma = 1$), $(dZ_t^a)^2 = dt$. ι_t^a is investment function of capital, and $\Phi(\iota_t^a)$ is a functional form for the investment function.

Rewrite the process of η_t as $d\eta_t = \mu_t^\eta \eta_t dt + \sigma_t^{\eta a} \eta_t dZ_t^a$. Then

$$\begin{aligned} (d\eta_t)^2 &= (\mu_t^\eta \eta_t dt + \sigma_t^{\eta a} \eta_t dZ_t^a)^2 \\ &= (\sigma_t^{\eta a} \eta_t)^2 dt + (\mu_t^\eta \eta_t)^2 (dt)^2 + 2(\mu_t^\eta \eta_t)(\sigma_t^{\eta a} \eta_t) dt dZ_t^a \\ &= (\sigma_t^{\eta a} \eta_t)^2 dt + o(dt), \end{aligned}$$

where $o(dt) = \{f : |f(\eta_t, t)| < \epsilon |dt|, \forall \epsilon > 0\}$.

The price is a process dependent of the state variable η_t , $q_t^a = q_t^a(\eta_t)$. By Ito's Lemma,

$$\begin{aligned} d(q_t^a(\eta_t)) &= \frac{\partial q_t^a}{\partial \eta_t} d\eta_t + \frac{1}{2} \frac{\partial^2 q_t^a}{\partial \eta_t^2} (d\eta_t)^2 \\ &= \frac{\partial q_t^a}{\partial \eta_t} (\mu_t^\eta \eta_t dt + \sigma_t^{\eta a} \eta_t dZ_t^a) + \frac{1}{2} \frac{\partial^2 q_t^a}{\partial \eta_t^2} (\sigma_t^{\eta a} \eta_t)^2 dt \\ &= \left(\frac{\partial q_t^a}{\partial \eta_t} \mu_t^\eta \eta_t + \frac{1}{2} \frac{\partial^2 q_t^a}{\partial \eta_t^2} (\sigma_t^{\eta a} \eta_t)^2 \right) dt + \frac{\partial q_t^a}{\partial \eta_t} \sigma_t^{\eta a} \eta_t dZ_t^a \end{aligned}$$

Match the terms with $\frac{dq_t^a}{q_t^a} = \mu_t^{qa} dt + \sigma_t^{qa} dZ_t^a$,

$$\begin{aligned} \mu_t^{qa} &= \frac{1}{q_t^a} \left(\frac{\partial q_t^a}{\partial \eta_t} \mu_t^\eta \eta_t + \frac{1}{2} \frac{\partial^2 q_t^a}{\partial \eta_t^2} (\sigma_t^{\eta a} \eta_t)^2 \right), \\ \sigma_t^{qa} &= \frac{1}{q_t^a} \frac{\partial q_t^a}{\partial \eta_t} \sigma_t^{\eta a} \eta_t. \end{aligned}$$

Similarly, ξ_t^j is a process dependent of η_t , $\xi_t^j = \xi_t^j(\eta_t)$. Matching terms with $\frac{d\xi_t^j}{\xi_t^j} = \mu_t^{\xi j} dt + \sigma_t^{\xi ja} dZ_t^a$,

$$\begin{aligned} \mu_t^{\xi j} &= \frac{1}{\xi_t^j} \left(\frac{\partial \xi_t^j}{\partial \eta_t} \mu_t^\eta \eta_t + \frac{1}{2} \frac{\partial^2 \xi_t^j}{\partial \eta_t^2} (\sigma_t^{\eta a} \eta_t)^2 \right), \\ \sigma_t^{\xi ja} &= \frac{1}{\xi_t^j} \frac{\partial \xi_t^j}{\partial \eta_t} \sigma_t^{\eta a} \eta_t. \end{aligned}$$

Using Ito's product rule, the process of the value of the capital $q_t^a k_t^a$ is

$$\begin{aligned} d(q_t^a k_t^a) &= q_t^a dk_t^a + k_t^a dq_t^a + dq_t^a dk_t^a, \\ \text{or } \frac{d(q_t^a k_t^a)}{q_t^a k_t^a} &= \frac{dk_t^a}{k_t^a} + \frac{dq_t^a}{q_t^a} + \frac{dq_t^a}{q_t^a} \frac{dk_t^a}{k_t^a} \\ &= (\mu^a + \Phi(\iota_t^a))dt + \sigma^a dZ_t^a + \mu_t^{qa} dt + \sigma_t^{qa} dZ_t^a + \sigma^a \sigma_t^{qa} dt + o(dZ_t^a) \\ &= (\mu^a + \Phi(\iota_t^a) + \mu_t^{qa} + \sigma^a \sigma_t^{qa})dt + (\sigma^a + \sigma_t^{qa})dZ_t^a, \end{aligned}$$

which is the capital gain rate.

Let α^a be the productivity rate. The dividend yield generated by the capital is $(\alpha^a - \iota_t^a)/q_t^a$. The return process is:

$$\begin{aligned} dr_t^{ka} &= \text{divident yield} + \text{capital gain rate} \\ &= \left(\underbrace{\mu^a + \Phi(\iota_t^a) + \mu_t^{qa} + \sigma^a \sigma_t^{qa} + \frac{\alpha^a - \iota_t^a}{q_t^a}}_{r_t^{ka}} \right) dt + (\sigma^a + \sigma_t^{qa})dZ_t^a. \end{aligned} \quad (11)$$

B.5.2 HJB Equation Optimality

Consider the following HJB equation:

$$\begin{aligned} 0 &= \sup_{w_t^{ja}, \iota_t^{ja}, c_t^j} f(c_t^j, U_t^j) + \mathbb{E}_t(dU_t^j) \\ &= \sup_{w_t^{ja}, \iota_t^{ja}, c_t^j} \left\{ \frac{f(c_t^j n_t^j, V_t^j)}{(\xi_t^j n_t^j)^{(1-\gamma^j)}} + \mu_t^{\xi j} + \mu_t^{nj} - \frac{\gamma^j}{2} (\sigma_t^{nja})^2 - \frac{\gamma^j}{2} (\sigma_t^{\xi ja})^2 + (1 - \gamma^j) \sigma_t^{\xi ja} \sigma_t^{nja} \right\}, \end{aligned} \quad (12)$$

where the normalized aggregator f follows the recursive utility:

$$f(c_t^j n_t^j, V_t^j) = \left(\frac{1 - \gamma^j}{1 - 1/\zeta^j} \right) \rho^j V_t^j \left[\left(\frac{c_t^j n_t^j}{[(1 - \gamma^j) V_t^j]^{1/(1-\gamma^j)}} \right)^{1-1/\zeta^j} - 1 \right]. \quad (13)$$

The agents have Epstein-Zin preferences [14]. The value function can be verified as

$$V_t^j = \frac{(n_t^j \xi_t^j)^{1-\gamma^j}}{1 - \gamma^j}. \quad (14)$$

The HJB equation can be rewritten as

$$\begin{aligned} &\frac{f(c_t^j n_t^j, V_t^j)}{(\xi_t^j n_t^j)^{(1-\gamma^j)}} + \mu_t^{\xi j} + \mu_t^{nj} - \frac{\gamma^j}{2} (\sigma_t^{nja})^2 - \frac{\gamma^j}{2} (\sigma_t^{\xi ja})^2 + (1 - \gamma^j) \sigma_t^{\xi ja} \sigma_t^{nja} \\ &= \frac{\rho^j}{1 - 1/\zeta^j} \left[\left(\frac{c_t^j}{\xi_t^j} \right)^{1-1/\zeta^j} - 1 \right] + \mu_t^{\xi j} + \mu_t^{nj} - \frac{\gamma^j}{2} (\sigma_t^{nja})^2 - \frac{\gamma^j}{2} (\sigma_t^{\xi ja})^2 + (1 - \gamma^j) \sigma_t^{\xi ja} \sigma_t^{nja}. \end{aligned}$$

Given $\mu_t^{nj} = r_t - c_t^j + w_t^{ja}(r_t^{ka} - r_t)$ and $\sigma_t^{nja} = w_t^{ja}(\sigma^a + \sigma_t^{qa})$ from the budget constraint:

$$\frac{dn_t^j}{n_t^j} = \left(\underbrace{r_t - c_t^j + w_t^{ja}(r_t^{ka} - r_t)}_{\mu_t^{nj}} \right) dt + \underbrace{w_t^{ja}(\sigma^a + \sigma_t^{qa})}_{\sigma_t^{nja}} dZ_t^a, \quad (15)$$

we get the HJB equation:

$$\begin{aligned}
F(w_t^{ja}, \iota_t^{ja}, c_t^j) &= \frac{\rho^j}{1 - 1/\zeta^j} \left[\left(\frac{c_t^j}{\xi_t^j} \right)^{1-1/\zeta^j} - 1 \right] + \mu_t^{\xi j} + r_t - c_t^j + w_t^{ja} (r_t^{ka} - r_t) \\
&\quad - \frac{\gamma^j}{2} (w_t^{ja})^2 (\sigma^a + \sigma_t^{qa})^2 - \frac{\gamma^j}{2} (\sigma_t^{\xi ja})^2 + (1 - \gamma^j) \sigma_t^{\xi ja} w_t^{ja} (\sigma^a + \sigma_t^{qa}) \\
&= \frac{\rho^j}{1 - 1/\zeta^j} \left[\left(\frac{c_t^j}{\xi_t^j} \right)^{1-1/\zeta^j} - 1 \right] + \mu_t^{\xi j} + r_t - c_t^j \\
&\quad + w_t^{ja} \left(\mu_t^{qa} + \mu^a + \Phi(\iota_t^a) + \sigma^a \sigma_t^{qa} + \frac{\alpha^a - \iota_t^a}{q_t^a} - r_t \right) \\
&\quad - \frac{\gamma^j}{2} (w_t^{ja})^2 (\sigma^a + \sigma_t^{qa})^2 - \frac{\gamma^j}{2} (\sigma_t^{\xi ja})^2 + (1 - \gamma^j) \sigma_t^{\xi ja} w_t^{ja} (\sigma^a + \sigma_t^{qa})
\end{aligned}$$

The first-order condition (FOC) of $F(w_t^{ja}, \iota_t^{ja}, c_t^j)$ requires $\nabla F(w_t^{ja}, \iota_t^{ja}, c_t^j) = \left(\frac{\partial F}{\partial w_t^{ja}}, \frac{\partial F}{\partial \iota_t^{ja}}, \frac{\partial F}{\partial c_t^j} \right)^T = 0$. This gives the necessary condition for optimality as:

$$\begin{aligned}
\frac{\partial F}{\partial w_t^{ja}} &= (r_t^{ka} - r_t) - \gamma^j w_t^{ja} (\sigma^a + \sigma_t^{qa})^2 + (1 - \gamma^j) \sigma_t^{\xi ja} (\sigma^a + \sigma_t^{qa}) = 0; \\
\frac{\partial F}{\partial \iota_t^{ja}} &= w_t^{ja} \left(\Phi'(\iota_t^a) - \frac{1}{q_t^a} \right) = 0; \\
\frac{\partial F}{\partial c_t^j} &= \frac{\rho^j}{1 - 1/\zeta^j} \frac{1}{(\xi_t^j)^{1-1/\zeta^j}} (1 - 1/\zeta^j) (c_t^j)^{-1/\zeta^j} - 1 = 0.
\end{aligned}$$

$$\frac{\partial F}{\partial w_t^{ja}} = 0 \text{ gives } (r_t^{ka} - r_t) - \gamma^j w_t^{ja} (\sigma^a + \sigma_t^{qa})^2 + (1 - \gamma^j) \sigma_t^{\xi ja} (\sigma^a + \sigma_t^{qa}) = 0.$$

$$\frac{\partial F}{\partial \iota_t^{ja}} = 0 \text{ while } w_t^{ja} \neq 0 \text{ gives } \Phi'(\iota_t^a) - \frac{1}{q_t^a} = 0.$$

$$\frac{\partial F}{\partial c_t^j} = 0 \text{ with } \zeta^j \approx 1 \text{ gives } \rho^j (c_t^j)^{-1} - 1 \approx 0, c_t^j \approx \rho^j.$$

We take the investment function as $\iota_t^a = \frac{q_t^a - 1}{\kappa}$. Then the functional form is $\Phi(\iota_t^a) = \frac{1}{\kappa} \log(1 + \kappa \iota_t^a)$.

We use agent h to compute r_t ,

$$r_t = r_t^{ka} - \gamma^h w_t^{ha} (\sigma^a + \sigma_t^{qa})^2 + (1 - \gamma^h) \sigma_t^{\xi ha} (\sigma^a + \sigma_t^{qa}). \quad (16)$$

Then add sentiment to agent i ,

$$r_t^{\hat{ka}} = r_t^{ka} + \frac{\mu^O - \mu^a}{\sigma^a} (\sigma^a + \sigma_t^{qa}). \quad (17)$$

It should satisfy the endogenous equation:

$$r_t^{\hat{ka}} - r_t = \gamma^i w_t^{ia} (\sigma^a + \sigma_t^{qa})^2 - (1 - \gamma^i) \sigma_t^{\xi ia} (\sigma^a + \sigma_t^{qa}). \quad (18)$$

B.5.3 Market Clearing Conditions

Consider the capital for each agent k_t^h and k_t^i , their sum should equal the total capital $k_t^h + k_t^i = k_t^a$. Also, the wealth share is defined as $\eta_t = \frac{n_t^i}{n_t^h + n_t^i}$. Total budget should equal total capital gain, so $n_t^h + n_t^i = q_t^a k_t^a$. Then

$$\eta_t = \frac{n_t^i}{n_t^h + n_t^i} = \frac{n_t^i}{q_t^a k_t^a}. \quad (19)$$

When market clears, quantity supplied is equal to the quantity demanded at the clearing price, and consumption from both types of agents equals surplus from the production.

$$\begin{aligned}
c_t^i n_t^i + c_t^h n_t^h &= (\alpha^a - \iota_t^a)(k_t^i + k_t^h) \\
c_t^i n_t^i + c_t^h n_t^h &= (\alpha^a - \iota_t^a)k_t^a \\
\frac{c_t^i n_t^i}{q_t^a k_t^a} + \frac{c_t^h n_t^h}{q_t^a k_t^a} &= \frac{\alpha^a - \iota_t^a}{q_t^a} \\
c_t^i \eta_t + c_t^h (1 - \eta_t) &= \frac{\alpha^a - \iota_t^a}{q_t^a}
\end{aligned}$$

Consider the portfolio weights $w_t^{ja} = \frac{k_t^j q_t^a}{n_t^j}$.

$$\begin{aligned}
k_t^i + k_t^h &= k_t^a \\
\frac{k_t^i}{k_t^a} + \frac{k_t^h}{k_t^a} &= 1 \\
\frac{k_t^i n_t^i q_t^a}{n_t^i q_t^a k_t^a} + \frac{k_t^h n_t^h q_t^a}{n_t^h q_t^a k_t^a} &= 1 \\
\frac{k_t^i q_t^a}{n_t^i} \eta_t + \frac{k_t^h q_t^a}{n_t^h} (1 - \eta_t) &= 1 \\
w_t^{ia} \eta_t + w_t^{ha} (1 - \eta_t) &= 1
\end{aligned}$$

Therefore, from market clearing conditions, we get two endogenous equations:

$$\alpha^a - \iota_t^a = (c_t^i \eta_t + c_t^h (1 - \eta_t)) q_t^a \quad (20)$$

$$1 = w_t^{ia} \eta_t + w_t^{ha} (1 - \eta_t) \quad (21)$$

B.5.4 Model Details

The definition of constant parameters are provided in Table 16 and the definition of variables are provided in Table 17.

Table 16: 1D Economic Model Constant Parameters

Parameter	Definition	Value
γ^j	relative risk aversion	$\gamma^i = 2.0, \gamma^h = 5.0$
ρ^j	discount rate	$\rho^i = \rho^h = 0.05$
ζ^j	intertemporal elasticity of substitution	$\zeta^i = \zeta^h = 1.00005$
μ^a	growth rate of capital	0.04
σ^a	volatility of capital	0.2
μ^O	sentiment factor	0.04
α^a	productivity	0.1
κ	investment cost	10000

Table 17: 1D Model Variables

Type	Definition
State Variables	$\eta_t (\eta)$
Agents	ξ_t^i, ξ_t^h
Endogenous Variables	$\mu_t^\eta, \sigma_t^{\eta^a}, q_t^a, w_t^{ia}, w_t^{ha}$

Equations to define new variables:

$$\iota_t^a = \frac{q_t^a - 1}{\kappa} \quad (22)$$

$$\Phi(\iota_t^a) = \frac{1}{\kappa} \log(1 + \kappa \iota_t^a) \quad (23)$$

$$c_t^j = (\rho^j)^{\zeta^j} (\xi_t^j)^{1-\zeta^j} \quad (24)$$

$$\sigma_t^{qa} = \frac{1}{q_t^a} \frac{\partial q_t^a}{\partial \eta_t} \sigma_t^{\eta a} \eta_t \quad (25)$$

$$\sigma_t^{nja} = w_t^{ja} (\sigma^a + \sigma_t^{qa}) \quad (26)$$

$$\sigma_t^{\xi ja} = \frac{1}{\xi_t^j} \frac{\partial \xi_t^j}{\partial \eta_t} \sigma_t^{\eta a} \eta_t \quad (27)$$

$$\sigma_t^{na} = \eta_t \sigma_t^{nia} + (1 - \eta_t) \sigma_t^{nha} \quad (28)$$

$$\mu_t^{qa} = \frac{1}{q_t^a} \left(\frac{\partial q_t^a}{\partial \eta_t} \mu_t^{\eta a} \eta_t + \frac{1}{2} \frac{\partial^2 q_t^a}{\partial \eta_t^2} (\sigma_t^{\eta a} \eta_t)^2 \right) \quad (29)$$

$$r_t^{ka} = \mu_t^{qa} + \mu^a + \Phi_t^a + \sigma^a \sigma^{qa} + \frac{\alpha^a - \iota_t^a}{q_t^a} \quad (30)$$

$$r_t = r_t^{ka} - \gamma^h w_t^{ha} (\sigma^a + \sigma_t^{qa})^2 + (1 - \gamma^h) \sigma_t^{\xi ha} (\sigma^a + \sigma_t^{qa}) \quad (31)$$

$$\mu_t^{nj} = r_t - c_t^j + w_t^{ja} (r_t^{ka} - r_t) \quad (32)$$

$$\mu_t^{\xi j} = \frac{1}{\xi_t^j} \left(\frac{\partial \xi_t^j}{\partial \eta_t} \mu_t^{\eta a} \eta_t + \frac{1}{2} \frac{\partial^2 \xi_t^j}{\partial \eta_t^2} (\sigma_t^{\eta a} \eta_t)^2 \right) \quad (33)$$

$$r_t^{\hat{ka}} = r_t^{ka} + \frac{\mu^O - \mu^a}{\sigma^a} (\sigma^a + \sigma_t^{qa}) \quad (34)$$

Endogenous equations to pin down endogenous variables:

$$\mu_t^{\eta} = (1 - \eta_t) (\mu_t^{ni} - \mu_t^{nh}) + (\sigma_t^{na})^2 - \sigma_t^{nia} \sigma_t^{na} \quad (35)$$

$$\sigma_t^{\eta a} = (1 - \eta_t) (\sigma_t^{nia} - \sigma_t^{nha}) \quad (36)$$

$$r_t^{\hat{ka}} - r_t = \gamma^i w_t^{ia} (\sigma^a + \sigma_t^{qa})^2 - (1 - \gamma^i) \sigma_t^{\xi ia} (\sigma^a + \sigma_t^{qa}) \quad (37)$$

$$1 = w_t^{ia} \eta_t + w_t^{ha} (1 - \eta_t) \quad (38)$$

$$\alpha^a - \iota_t^a = (c_t^i \eta_t + c_t^h (1 - \eta_t)) q_t^a \quad (39)$$

HJB equations to solve for agent value functions:

$$0 = \frac{\rho^i}{1 - \frac{1}{\zeta^i}} \left(\left(\frac{c_t^i}{\xi_t^i} \right)^{1-1/\zeta^i} - 1 \right) + \mu_t^{\xi i} + \mu_t^{ni} - \frac{\gamma^i}{2} (\sigma_t^{nia})^2 - \frac{\gamma^i}{2} (\sigma_t^{\xi ia})^2 + (1 - \gamma^i) \sigma_t^{\xi ia} \sigma_t^{nia} \quad (40)$$

$$0 = \frac{\rho^h}{1 - \frac{1}{\zeta^h}} \left(\left(\frac{c_t^h}{\xi_t^h} \right)^{1-1/\zeta^h} - 1 \right) + \mu_t^{\xi h} + \mu_t^{nh} - \frac{\gamma^h}{2} (\sigma_t^{nha})^2 - \frac{\gamma^h}{2} (\sigma_t^{\xi ha})^2 + (1 - \gamma^h) \sigma_t^{\xi ha} \sigma_t^{nha} \quad (41)$$

B.5.5 Results

The agents and endogenous variables are configured as 4-layer MLPs with 30 hidden units per layer and tanh activation. ξ_t^i , ξ_t^h , and q_t^a are constrained by SoftPlus (a smooth approximation to the ReLU function) to ensure positive outputs, thereby guaranteeing that the price of capital and agent wealth remain non-negative. The state variable η_t is restricted to $[0.01, 0.99]$ to avoid instabilities at extreme share holdings. The system is trained for 2000 epochs using Adam optimizer with a learning rate of 10^{-3} , under the endogenous and HJB constraints. As the share of wealth held by agent i (η_t) increases, so does the price of capital q_t^a . The growth rate for capital price is decreasing, indicating diminishing returns. The volatility of the price, represented by σ_t^{qa} , peaks when η_t is around $0.3 \sim 0.4$, reflecting the highest uncertainty. At extreme points, $\eta_t \rightarrow 0$ or $\eta_t \rightarrow 1$, $\sigma_t^{qa} \rightarrow 0$, indicating minimal price uncertainty when one type of

agent holds all the wealth. Both agents maintain a long position, as evidenced by the positive portfolio weights w_t^{ia} and w_t^{ha} . When $\eta_t \sim 0$, only agent h is contributing to the total capital, resulting in $w_t^{ha}(0) = 1$. As η_t increases, both weights decrease, with w_t^{ia} decreasing more rapidly (from 2 to 1) than w_t^{ha} (from 1 to 0.3). This ensures the market clearing condition, where the weighted sum of the capital portfolio held by intermediary i and household h always equals the total capital k_t^a . Figure 12 shows the results.

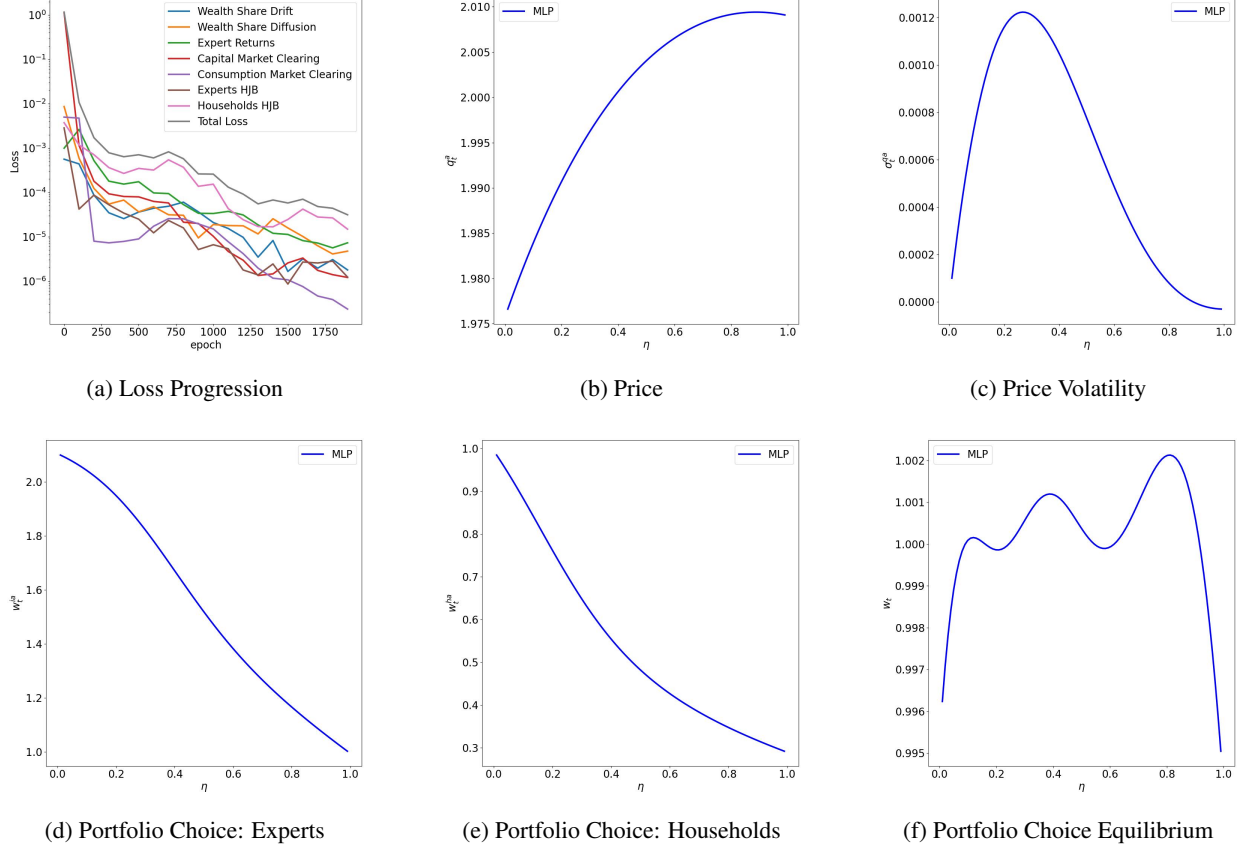


Figure 12: One-Dimensional Model Results

B.6 Variable Parameters and Inverse Problems

Consider the single-asset two-dimensional Black-Scholes equation. We are interested in finding solutions for various parameter values. To achieve this, we treat the parameters as pseudo state variables and include them as neural network inputs. This approach increases the dimensionality and complexity of the problem. However, once the neural network is trained, the solution becomes available for any point in the state and parameter spaces. Specifically, we solve the following four-dimensional problem with state variables $(S, t, \sigma, r) \in [0, 1] \times [0, 1] \times [0.1, 0.3] \times [0.01, 0.1]$:

$$\begin{aligned} \frac{\partial V}{\partial t} + rS \frac{\partial V}{\partial S} + \frac{\sigma^2}{2} S^2 \frac{\partial^2 V}{\partial S^2} - rV &= 0, \\ V(S, T) &= \max\{S - K, 0\} \end{aligned}$$

Figure 13a illustrates the model fit for two parameter sets: $(\sigma = 0.2, r = 0.01)$ and $(\sigma = 0.1, r = 0.1)$, using a 4-Layer MLP with SiLU activation (2971 parameters). The MSEs are 1.50×10^{-5} and 2.59×10^{-5} respectively.

In some cases, the parameters themselves may be unknown, but partial observations are available. To address this, we can simultaneously solve for the exact solution and approximate the corresponding parameters. For instance, we set the ground truth values to $\sigma = 0.2$ and $r = 0.05$, with initial parameter guesses of $\hat{\sigma} = 0.15$ and $\hat{r} = 0.04$. The fit results are shown in Figure 13b. The parameters approximated by the MLP are $\sigma = 0.19$ and $r = 0.05$, while those approximated by the KAN are $\sigma = -0.1$ and $r = 0.06$.

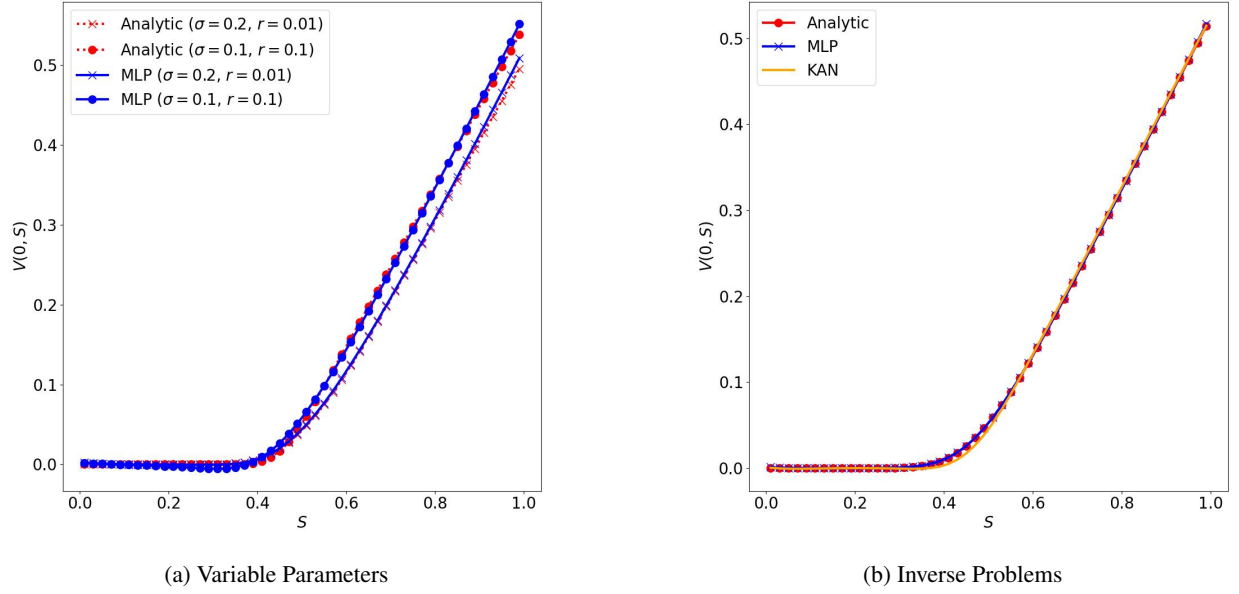


Figure 13: In (a), the fit of MLP (blue) models are shown for several parameters. The analytic solutions are plotted in red. In (b), the fit of MLP and KAN for the inverse problems are plotted against the analytic solution.